


## Decoding polymer self-dynamics using a two-step approach

Zhiqiang Shen , Jan-Michael Y. Carrillo , Bobby G. Sumpter , and Yangyang Wang <sup>\*</sup>  
 Center for Nanophase Materials Sciences, Oak Ridge National Laboratory, Oak Ridge, Tennessee 37831, USA

 (Received 19 April 2022; accepted 22 June 2022; published 11 July 2022)

The self-correlation function and corresponding self-intermediate scattering function in Fourier space are important quantities for describing the molecular motions of liquids. This work draws attention to a largely overlooked issue concerning the analysis of these space-time density-density correlation functions of polymers. We show that the interpretation of non-Gaussian behavior of polymers is generally complicated by intrachain averaging of distinct self-dynamics of different segments. By the very nature of the mathematics involved, the averaging process not only conceals critical dynamical information, but also contributes to the observed non-Gaussian dynamics. To fully expose this issue and provide a thorough benchmark of polymer self-dynamics, we perform analyses of coarse-grained molecular dynamics simulations of linear and ring polymer melts as well as several theoretical models using a “two-step” approach, where interchain and intrachain averagings of segmental self-dynamics are separated. While past investigations primarily focused on the average behavior, our results indicate that a more nuanced approach to polymer self-dynamics is clearly required.

DOI: [10.1103/PhysRevE.106.014502](https://doi.org/10.1103/PhysRevE.106.014502)

### I. INTRODUCTION

Brownian motions are an important facet of polymeric liquid dynamics. According to the classical theory [1,2], a Brownian motion starting from the origin at time  $t = 0$  is characterized by a Gaussian spatiotemporal probability density function (PDF)  $G_s(\mathbf{r}, t)$  [3]:

$$G_s(\mathbf{r}, t) = \frac{1}{(4\pi Dt)^{3/2}} \exp\left(-\frac{\mathbf{r}^2}{4Dt}\right), \quad (1)$$

where  $D$  is the diffusivity and  $\mathbf{r}$  is the position of the particle. And the corresponding mean-squared displacement ( $\langle \mathbf{r}^2(t) \rangle$ ) (MSD) has a linear time dependence:

$$\langle \mathbf{r}^2(t) \rangle = \int \mathbf{r}^2 G_s(\mathbf{r}, t) d\mathbf{r} = 6Dt. \quad (2)$$

It is well known that deviations from this classical example often occur in polymeric materials [4]. Anomalous, subdiffusive behavior of polymer melts has been widely observed and extensively studied by experiments [5–9], theories [4,10–13], and computer simulations [14–18]. While significant attention has been given to the segmental or center-of-mass (c.m.) mean-squared displacement in these studies, the underlying probability density function (self-correlation function), which contains crucial information about polymer real-space self-dynamics, has received little scrutiny. In particular, despite some sporadic discussions, there are no systematic investigations about the non-Gaussian (sub)diffusion behavior of polymer melts at temperatures *far above the glass transition*. The current study attempts to fill in this gap by detailed analysis of molecular dynamics simulations. Recently, we presented a comprehensive analysis of spatial correlations of polymer dynamics in the reciprocal space [19]. The current

work turns attention to the real-space dynamics, with the focus on the self-correlation functions. Properly addressing polymer melt self-dynamics, however, requires attention to a more general and largely overlooked issue concerning the computation of self-correlation and self-intermediate scattering functions of polymers.

The self-correlation function (self-part of the van Hove function) [20–22]  $G_s(\mathbf{r}, t)$  of a particle system, often in the context of molecular dynamics simulations, can be computed as follows:

$$G_s(\mathbf{r}, t) = \frac{1}{N_{\text{total}}} \sum_{i=1}^{N_{\text{total}}} \langle \delta\{\mathbf{r} - [\mathbf{r}_i(t + t') - \mathbf{r}_i(t')]\} \rangle, \quad (3)$$

where  $N_{\text{total}}$  is the total number of particles,  $\mathbf{r}_i(t)$  is the position the  $i$ th particle at time  $t$ , and  $\langle \dots \rangle$  stands for proper ensemble and time averagings. For the sake of simplicity, we set  $t' = 0$  from this point onward in our discussions. The corresponding self-intermediate scattering function  $F_s(\mathbf{Q}, t)$  is

$$\begin{aligned} F_s(\mathbf{Q}, t) &= \int G_s(\mathbf{r}, t) e^{-i\mathbf{Q}\cdot\mathbf{r}} d\mathbf{r} \\ &= \frac{1}{N_{\text{total}}} \sum_{i=1}^{N_{\text{total}}} \langle \exp\{i\mathbf{Q} \cdot [\mathbf{r}_i(t) - \mathbf{r}_i(0)]\} \rangle, \end{aligned} \quad (4)$$

with  $\mathbf{Q}$  being the scattering wave vector. Without question, Eqs. (3) and (4) should be applicable to both atomic and polymeric liquids. However, as we shall explain in detail in Sec. II, the interchain and intrachain averaging processes in Eqs. (3) and (4) bury important information of *polymer* self-dynamics. In particular, the non-Gaussian parameter  $\alpha_2(t)$ , defined by the second and fourth moments of  $G_s(\mathbf{r}, t)$ ,

$$\alpha_2(t) = \frac{3 \int \mathbf{r}^4 G_s(\mathbf{r}, t) d\mathbf{r}}{5 \left[ \int \mathbf{r}^2 G_s(\mathbf{r}, t) d\mathbf{r} \right]^2} - 1 = \frac{3 \langle [\mathbf{r}_i(t) - \mathbf{r}_i(0)]^4 \rangle}{5 \langle [\mathbf{r}_i(t) - \mathbf{r}_i(0)]^2 \rangle^2} - 1, \quad (5)$$

<sup>\*</sup>wangy@ornl.gov

can be strongly affected, producing a somewhat distorted view of the non-Gaussian displacement at the segmental level. Concrete arguments and examples supporting the above statements will be supplied in Secs. II and III. To dissect the self-dynamics defined by Eqs. (3), we perform analyses of theories and simulations using a “two-step” approach, where interchain and intrachain averagings of segmental motions are separated. In doing so, this study provides a thorough characterization of polymer melt self-dynamics in *real space*.

To place the results reported herein in the context of other related studies, two comments are in order. First, the main objective of our investigation is to analyze the real-space self-dynamics of polymers at relatively large length scales and long timescales, and at temperatures well above the glass transition. Instead of focusing on the  $\alpha$  relaxation [23–27], the current analysis is concerned with the non-Gaussian behavior of slow polymer melt dynamics. On the other hand, an intriguing question is to what a degree the techniques developed for glassy liquids [28–30] can be applied to study the heterogeneities in polymer melt dynamics at high temperatures [31,32]. Second, while previous neutron spin-echo spectroscopy (NSE) experiments and computer simulations have suggested non-Gaussian self-dynamics in both linear and ring polymers [33–36], the molecular origin of these observations is yet to be clarified. In particular, the influences of entanglement and chain architecture on the functional form of the self-correlation function  $G_s(\mathbf{r}, t)$  have not been systematically explored. Using a B-spline fitting algorithm based on squared distance minimization [37], single-molecule fluorescence imaging experiments of entangled F-actin solutions demonstrated that the probability density function of segmental displacement perpendicular to the tube axis  $G_s(r_\perp, t)$  exhibits an exponential tail, which can be further linked to the anharmonicity of the tube confining potential [8]. Nevertheless, a general knowledge about the self-correlation function of entangled polymers is still not available, despite our recent analysis of intermediate scattering functions in the reciprocal space [19].

On the technical side, polymer self-motions on relatively short time and length scales can be experimentally probed by quasielastic neutron scattering [38–40]. However, accessing melt self-dynamics at longer time and length scales has remained challenging for inelastic neutron scattering techniques [7,41]. Therefore, this work employs coarse-grained molecular dynamics simulations to computationally explore the self-dynamics of linear and ring polymer melts of different degrees of polymerization, at temperatures well above the glass transition. As stated above, a key idea of our analysis is to adopt a two-step approach to polymer self-dynamics. Specifically, we *explicitly* consider the self-correlation function  $G_s(\mathbf{r}, t)$  as an *intrachain* average of the segmental self-correlation function  $G_s(\mathbf{r}, t; i)$ , with  $G_s(\mathbf{r}, t; i)$  being an *interchain* average of the probability density distribution of displacement of segment  $i$  at correlation time  $t$ . Such a separation of intrachain and interchain averagings is critical for a lucid understanding of non-Gaussian self-dynamics in polymers.

Before diving into the detailed description of our methods and results, it is helpful to say a few words about the term “heterogeneity,” which we shall use in this paper. The concept

of heterogeneity is frequently invoked in studies of dynamics of glassy liquids [42–44]. Here we apply this concept in the narrow context of a non-Gaussian self-correlation function, where a heavy tail is observed. This type of non-Gaussian probability density function implies a broader distribution of particle displacement, relative to the Gaussian distribution. In a simplified picture, this amounts to the existence of fast- and slow-moving particles [30,43,45]. It is in this context that we shall discuss the heterogeneities of polymer melt self-dynamics.

## II. A TWO-STEP APPROACH TO POLYMER SELF-DYNAMICS

### A. Description of the method

To properly understand the self-dynamics of polymers, it is helpful to separate the interchain and intrachain averaging processes in computing the self-correlation function. Let us consider a polymer melt consisting of  $M$  chains, each with  $N$  segments (beads), the self-correlation function  $G_s(\mathbf{r}, t)$  for the entire system can be explicitly written as

$$\begin{aligned} G_s(\mathbf{r}, t) &= \frac{1}{N} \frac{1}{M} \sum_{i=1}^N \sum_{\alpha=1}^M \langle \delta \{ \mathbf{r} - [\mathbf{r}_i^\alpha(t) - \mathbf{r}_i^\alpha(0)] \} \rangle \\ &= \frac{1}{N} \sum_{i=1}^N G_s(\mathbf{r}, t; i), \end{aligned} \quad (6)$$

where  $\mathbf{r}_i^\alpha(t)$  is the position of segment  $i$  of chain  $\alpha$  at time  $t$  and  $G_s(\mathbf{r}, t; i)$  is the self-correlation of segment  $i$  defined as

$$G_s(\mathbf{r}, t; i) \equiv \frac{1}{M} \sum_{\alpha=1}^M \langle \delta \{ \mathbf{r} - [\mathbf{r}_i^\alpha(t) - \mathbf{r}_i^\alpha(0)] \} \rangle. \quad (7)$$

It is easy to see that  $G_s(\mathbf{r}, t)$  is the intrachain average of the segment dependent self-correlation function  $G_s(\mathbf{r}, t; i)$ , whereas  $G_s(\mathbf{r}, t; i)$  is the interchain average of the probability density distribution of displacement of segment  $i$ . This decomposition of the interchain and intrachain averaging processes is schematically illustrated in Fig. 1. Obviously, for such a decomposition to be meaningful, a consistent segment labeling scheme for all chains is required. The benefit of explicit consideration of  $G_s(\mathbf{r}, t; i)$  is twofold: on the one hand, it permits investigations of self-dynamics on the individual segment level; on the other hand, it also affords the opportunity to explore the heterogeneity of self-dynamics at the chain level.

Similarly, the total segment mean-squared displacement in the laboratory frame  $g_1(t)$  [14] can be decomposed based on the two-step approach as

$$\begin{aligned} g_1(t) &= \int G_s(\mathbf{r}, t) \mathbf{r}^2 d\mathbf{r} \\ &= \frac{1}{N} \frac{1}{M} \sum_{i=1}^N \sum_{\alpha=1}^M \langle [\mathbf{r}_i^\alpha(t) - \mathbf{r}_i^\alpha(0)]^2 \rangle \\ &= \frac{1}{N} \sum_{i=1}^N g_1(t; i), \end{aligned} \quad (8)$$

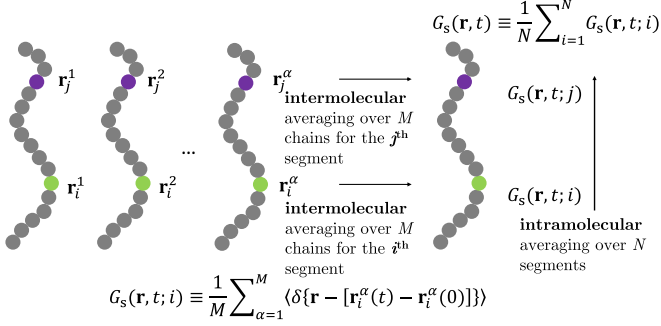


FIG. 1. Schematic illustration of the interchain and intrachain averaging processes in computing the average self-correlation function  $G_s(\mathbf{r}, t)$ . First, the distribution of displacement  $\langle \delta\{\mathbf{r} - [\mathbf{r}_i^\alpha(t) - \mathbf{r}_i^\alpha(0)]\} \rangle$  is averaged over  $M$  chains for the  $i$ th segment. This interchain averaging yields the self-correlation function  $G_s(\mathbf{r}, t; i)$ . Next, the self-correlation function  $G_s(\mathbf{r}, t; i)$  is averaged over  $N$  segments (intramolecular averaging), producing  $G_s(\mathbf{r}, t)$ . Note that a consistent segment labeling scheme is used for all chains.

with

$$g_1(t; i) \equiv \int G_s(\mathbf{r}, t; i) \mathbf{r}^2 d\mathbf{r} = \frac{1}{M} \sum_{\alpha=1}^M \langle [\mathbf{r}_i^\alpha(t) - \mathbf{r}_i^\alpha(0)]^2 \rangle. \quad (9)$$

$g_1(t; i)$  is the interchain average of mean-squared displacement for segment  $i$  and  $g_1(t)$  is the intrachain average of  $g_1(t; i)$ . Such an idea was touched upon in a previous computational investigation of entangled polymer dynamics [17], but has not been explored systematically in general.

From the self-correlation function  $G_s(\mathbf{r}, t; i)$ , the non-Gaussian parameter  $\alpha_2(t; i)$  for each segment  $i$  can be computed as

$$\begin{aligned} \alpha_2(t; i) &= \frac{3 \left\{ \frac{1}{M} \sum_{\alpha=1}^M \langle [\mathbf{r}_i^\alpha(t) - \mathbf{r}_i^\alpha(0)]^4 \rangle \right\}}{5 \left\{ \frac{1}{M} \sum_{\alpha=1}^M \langle [\mathbf{r}_i^\alpha(t) - \mathbf{r}_i^\alpha(0)]^2 \rangle \right\}^2} - 1 \\ &= \frac{3 \int \mathbf{r}^4 G_s(\mathbf{r}, t; i) d\mathbf{r}}{5 \left[ \int \mathbf{r}^2 G_s(\mathbf{r}, t; i) d\mathbf{r} \right]^2} - 1. \end{aligned} \quad (10)$$

It is important to realize that the commonly used non-Gaussian parameter  $\alpha_2(t)$  defined by Eq. (5) is not a simple arithmetic average of  $\alpha_2(t; i)$ :  $\alpha_2(t) \neq N^{-1} \sum_{i=1}^N \alpha_2(t; i)$ . In fact, it is possible to have  $\alpha_2(t) > 0$  with  $\alpha_2(t; i) = 0$  for each segment, as in the case for the Rouse model. This simple mathematical fact implies that the intrachain averaging process of self-dynamics may engender non-Gaussian behavior in the average self-correlation function  $G_s(\mathbf{r}, t)$  and the corresponding parameter  $\alpha_2(t)$ .

The proposed “two-step” approach is a natural way of thinking about polymer self-dynamics. However, previous investigations have primarily focused on the average density-density self-correlations in real [ $G_s(\mathbf{r}, t)$ ] and reciprocal spaces [ $F_s(\mathbf{Q}, t)$ ], as well as the corresponding  $g_1(t)$ , and  $\alpha_2(t)$ . The new method helps to clarify the molecular origin of non-Gaussian behavior of polymers, by providing a close view of self-dynamics at two levels. The self-dynamics at the *segment level* is characterized by  $G_s(\mathbf{r}, t; i)$ , which is the interchain average of the probability density distribution of

displacement of segment  $i$ . As shall be demonstrated, constrained molecular motions in polymers (e.g., reptation, as opposed to free Rouse motions) produce an exponential tail in  $G_s(\mathbf{r}, t; i)$ , resulting in non-Gaussian behavior. Additionally, similar to the case of atomic fluids, non-Gaussianity in  $G_s(\mathbf{r}, t; i)$  can also arise from “intermolecular heterogeneities” in polymer self-dynamics. For long chains, such heterogeneities may come from local fluctuations of entanglement constraints. At the *chain level*, variations of  $G_s(\mathbf{r}, t; i)$  among different segments can give rise to non-Gaussian behavior as well. This may be regarded as “intramolecular heterogeneity” in polymer self-dynamics. Supporting evidence of the above statements is given in the following subsection and in Sec. III.

### B. Application to theoretical models

To see the benefits of the two-step approach, let us first recall some well-known results of the Rouse model [46]. The model predicts that the mean-squared displacement  $g_{1,\text{linear}}(t; i)$  of segment  $i$  of a linear chain, defined by Eq. (9), is described by the following equation [4]:

$$\begin{aligned} g_{1,\text{linear}}(t; i) &= 6D_G t + \frac{4Nb^2}{\pi^2} \left\{ \sum_{p=1}^{\infty} \frac{1}{p^2} \cos^2 \left( \frac{p\pi i}{N} \right) \right. \\ &\quad \left. \times [1 - \exp(-t p^2 / \tau_{R,\text{linear}})] \right\}, \end{aligned} \quad (11)$$

where  $D_G$  is the center-of-mass diffusion coefficient,  $N$  is the number of segments (beads) in a chain,  $b$  is the segment size, and  $\tau_{R,\text{linear}}$  is the Rouse relaxation time. In the long-time limit, the center-of-mass diffusion dominates, and  $g_1(t; i)$  is insensitive to the position of the segment in the chain. On short timescales ( $t \ll \tau_R$ ), however, the second term of Eq. (11) takes over and  $g_1(t; i)$  is strongly dependent on segment position  $i$ .

On the other hand, the self-intermediate scattering function  $F_s(\mathbf{Q}, t)$  of the Rouse model is given by

$$\begin{aligned} F_s(\mathbf{Q}, t) &= \frac{1}{N} \sum_{i=1}^N \langle \exp\{i\mathbf{Q} \cdot [\mathbf{r}_i(t) - \mathbf{r}_i(0)]\} \rangle \\ &= \frac{1}{N} \sum_{i=1}^N F_s(\mathbf{Q}, t; i) \\ &= \frac{1}{N} \sum_{i=1}^N \exp \left[ -\frac{1}{6} \mathbf{Q}^2 g_{1,\text{linear}}(t; i) \right], \end{aligned} \quad (12)$$

where  $F_s(\mathbf{Q}, t; i) \equiv \langle \exp\{i\mathbf{Q} \cdot [\mathbf{r}_i(t) - \mathbf{r}_i(0)]\} \rangle$  is the self-intermediate scattering function for segment  $i$ . The dynamic Gaussian approximation [4] is used for each  $F_s(\mathbf{Q}, t; i)$  in the derivation of the last equality of Eq. (12). While we are not aware of a strict theoretical justification for invoking the Gaussian approximation, the validity of this assumption can be shown numerically by Brownian dynamics simulations. In other words, the Rouse model yields Gaussian self-dynamics for each segment  $i$ . It is important to recognize that although each self-intermediate scattering function  $F_s(\mathbf{Q}, t; i)$  in Eq. (12) is Gaussian, the corresponding arithmetic average  $F_s(\mathbf{Q}, t)$  is *weakly non-Gaussian* for a linear chain, due to the

variation of segment mean-squared displacement  $g_1(t; i)$  [47]. Since the Fourier transform of a Gaussian function is still a Gaussian function, the self-correlation function  $G_s(\mathbf{r}, t)$  of the Rouse model is given by

$$\begin{aligned} G_s(\mathbf{r}, t) &= \frac{1}{N} \sum_{i=1}^N G_s(\mathbf{r}, t; i) \\ &= \frac{1}{N} \sum_{i=1}^N \left( \frac{3}{2\pi g_{1,\text{linear}}(t; i)} \right)^{3/2} \\ &\quad \times \exp\left( -\frac{3\mathbf{r}^2}{2g_{1,\text{linear}}(t; i)} \right). \end{aligned} \quad (13)$$

Similarly, while the self-correlation  $G_s(\mathbf{r}, t; i)$  of each segment  $i$  takes the form of a Gaussian function, the averaged self-correlation  $G_s(\mathbf{r}, t)$  is non-Gaussian for a linear chain: *the arithmetic average of Gaussian functions with different variances is non-Gaussian*. In the language of dynamic heterogeneity [43], which is narrowly defined in the Introduction, we may say that the non-Gaussian behavior of the Rouse model originates from intrachain heterogeneity of self-dynamics. We note that the *weak* non-Gaussian feature of self-dynamics in the Rouse model is not widely recognized in the literature. Further discussions of this issue can be found in Sec. III and Appendix B.

The tube model of Doi and Edwards paints a different picture for the self-intermediate scattering function of entangled polymers. Specifically, it predicts that the  $F_s(\mathbf{Q}, t; i)$  of each reptating chain segment  $i$  is described by the following equation [4,48]:

$$\begin{aligned} F_s(\mathbf{Q}, t; i) &= \sum_{p=1}^{\infty} \left\{ \frac{2\mu}{\mu^2 + \alpha_p^2 + \mu} \cos^2 \left[ \frac{2\alpha_p}{L} \left( s_i - \frac{L}{2} \right) \right] \right. \\ &\quad \times \exp\left( -\frac{4\alpha_p^2 t}{\pi^2 \tau_d} \right) \\ &\quad + \frac{2\mu}{\mu^2 + \beta_p^2 + \mu} \sin^2 \left[ \frac{2\beta_p}{L} \left( s_i - \frac{L}{2} \right) \right] \\ &\quad \left. \times \exp\left( -\frac{4\beta_p^2 t}{\pi^2 \tau_d} \right) \right\}, \end{aligned} \quad (14)$$

where  $\mu = \frac{1}{2} Q^2 R_G^2$ , with  $R_G$  being the radius of gyration,  $s_i$  is the curvilinear segment index which lies between 0 and the contour length  $L$ ,  $\tau_d$  is the reptation (disengagement) time, and  $\alpha_p$  and  $\beta_p$  are the solutions of the equations  $\alpha_p \tan \alpha_p = \mu$  and  $\beta_p \cot \beta_p = -\mu$ . In contrast to the Rouse model, the tube model envisions intrinsic non-Gaussian self-correlation for each segment  $i$ . The average self-intermediate scattering function  $F_s(\mathbf{Q}, t)$ , not surprisingly, is also non-Gaussian [4,19,48,49], which has been examined in detail in our previous study [19]. The mean-squared displacement of each segment  $g_1(t; i)$  is given by [4,48]

$$\begin{aligned} g_1(t; i) &= \frac{2Dt}{Z} + \frac{4Nb^2}{\pi^2} \sum_{p=1}^{\infty} \frac{1}{p^2} \\ &\quad \times \cos^2 \left( \frac{p\pi s_i}{L} \right) [1 - \exp(-t p^2 / \tau_d)], \end{aligned} \quad (15)$$

with  $D$  being the curvilinear diffusion coefficient and  $Z$  the number of entanglements per chain. Eq. (15) has the same mathematical structure as Eq. (11), although this is not necessarily a profound result [48]. At short time ( $t \ll \tau_d$ ), the second term of Eq. (15) dominates and  $g_1(t; i)$  varies strongly with  $i$ . Therefore, unlike the case of the Rouse model, the non-Gaussian behavior in the tube model has two contributing factors: the intrinsic non-Gaussian behavior of each segment and the variation of self-dynamics (mobility) within a chain.

The preceding analyses of the Rouse and tube models show that the proposed two-step method is an effective and natural approach to polymer self-dynamics. Nevertheless, existing computational studies have directed attention only to the averaged response [e.g.,  $g_1(t)$ ,  $F_s(\mathbf{Q}, t)$ , and  $\alpha_2(t)$ ], without a proper nuanced consideration at the molecular level [33,34,50–54]. While polymer  $\alpha$  relaxation is not the focus of the present investigation, the two-step analysis should be equally applicable to this problem. It is well known that the so-called chain-end effect plays an important role in the glass transition phenomenon of polymers [55,56]. The short-time self-dynamics of polymers (on the timescale of  $\tau_\alpha$ ), therefore, should generally depend on the relative position of the segment within a chain. An illustration of two-step analysis for the polymer  $\alpha$  relaxation problem will be provided towards the end of this paper.

Having laid down the basic idea of the two-step approach, we proceed to perform a thorough examination of the self-dynamics of linear and ring polymer melts, using coarse-grained molecular dynamics simulations of a semiflexible bead-spring model with purely repulsive interactions [18,57,58]. The results are analyzed and interpreted with the two-step method, and compared with several theoretical models including the Rouse model, the classical tube model, and the slip-spring model. The main objective of this exercise is to provide a detailed characterization of the real-space self-dynamics of polymer melts, through the lens of the segment dependent self-correlation function  $G_s(\mathbf{r}, t; i)$ , the corresponding mean-squared displacement  $g_1(t; i)$ , and the non-Gaussian parameter  $\alpha_2(t; i)$ . As indicated in the Introduction, the  $\alpha$  relaxation of polymers is not the focus of the current investigation. The short-time behavior is therefore not shown for the most part. Nevertheless, to demonstrate the potential applications of the two-step approach to glassy dynamics, molecular dynamics simulations of a coarse-grained bead-spring model with attractive interactions are briefly discussed as an example at the end of Sec. III. The details of our computational investigations, which include both molecular dynamics (MD) and Brownian dynamics (BD) simulations, are provided in Appendix A.

To properly compare the behavior of polymers of different degrees of polymerization (chain length)  $N$ , we adopt normalized segment indices in our analysis:

$$i^* \equiv \frac{i}{N}. \quad (16)$$

In the case of the classical tube theory,  $i^* \equiv s_i/L$ . Additionally, the segments in a linear chain are labeled sequentially from one end to another ( $i = 1, 2, \dots, N$ ), which is the most natural choice.

### III. RESULTS AND DISCUSSION

This section is organized as follows. The basic phenomenology of real-space self-dynamics of linear and ring polymers from molecular dynamics simulations will first be described in terms of the conventional, average self-correlation function  $G_s(\mathbf{r}, t)$ , mean-squared displacements [ $g_1(t)$  and  $g_3(t)$ ], and non-Gaussian parameter  $\alpha_2(t)$ . Next, the two-step approach is applied to analyze the origin of the observed non-Gaussian behavior. The third part of this section presents a comparison of the real-space self-dynamics from simulations with those from several theoretical models, including the Rouse model, the classical tube model, and the slip-spring model. Lastly, application of the two-step approach to polymer glassy dynamics is briefly discussed.

#### A. Basic phenomenology of average self-dynamics

Coarse-grained linear and ring polymers of five different degrees of polymerization  $N = 20, 40, 100, 300,$  and  $500$  were investigated by molecular dynamics simulations at  $\rho = 0.85 \sigma^{-3}$  and  $T = 1.0$ . It is worth noting that the Rouse time follows the scaling relations  $\tau_{R,\text{linear}} = \tau_0 N^2$  for linear chains and  $\tau_{R,\text{ring}} = \tau_0 N^2/4$  for rings, where  $\tau_0$  is the elementary relaxation time of a Rouse segment. Additionally, the entanglement equilibration time of a linear chain can be evaluated as  $\tau_e = \tau_0 N_e^2$ , where the number of beads between entanglements  $N_e \approx 28$  for the current model and  $\tau_0 \approx 2.58\tau$  with  $\tau = \sigma\sqrt{m/\epsilon}$  being the Lennard-Jones (LJ) time (see Appendix A for details). Figure 2 shows the general features of the average self-correlation functions  $G_s(r, t)$  from the simulations. To guide the interpretation of data, Gaussian distributions of  $[3/(2\pi g_1)]^{3/2} \exp[-3r^2/(2g_1)]$  are presented as references for  $G_s(r, t)$  at different correlation times. For the unentangled linear chains of  $N = 20$  and  $N = 40$ , their self-correlation functions  $G_s(r, t)$  exhibit weak deviations from the Gaussian reference curves at short times ( $t \lesssim \tau_R$ ) and become Gaussian only when the correlation time is much longer than the Rouse relaxation time (e.g.,  $t = 10\tau_R$ ). The self-correlation functions  $G_s(r, t)$  of the long linear chains of  $N = 300$  and  $N = 500$ , on the other hand, show substantial deviations from the Gaussian distributions on intermediate timescales ( $t \approx 0.1\tau_R$  and  $\tau_R$ ). The entanglement equilibration time  $\tau_e$  of these two systems is on the order of  $0.01\tau_R$ . Therefore, the strong non-Gaussian behavior occurs when  $t \gg \tau_e$ . To better illustrate the “fat” exponential-like tail of the non-Gaussian distribution, the normalized self-correlation functions are presented in the insets of Fig. 2, where  $r$  and  $G_s(r, t)$  are scaled by  $\sqrt{g_1}$  and  $[3/(2\pi g_1)]^{3/2}$ , respectively. In contrast to the behavior of the linear chains, the  $G_s(r, t)$  of ring polymers are largely Gaussian regardless of chain length. Only very weak deviations are observed in rings of  $N = 300$  and  $N = 500$ .

To further quantify the self-dynamics of linear and ring polymers, we compute the mean-squared displacements [ $g_1(t)$  and  $g_3(t)$ ] and non-Gaussian parameters  $\alpha_2(t)$  for both the segment and center of mass. The mean-squared displacement data in Figs. 3(a) and 3(b) show that the ring polymers move faster than their linear counterparts of the same length  $N$ , which is in line with previous MD simulations [57].

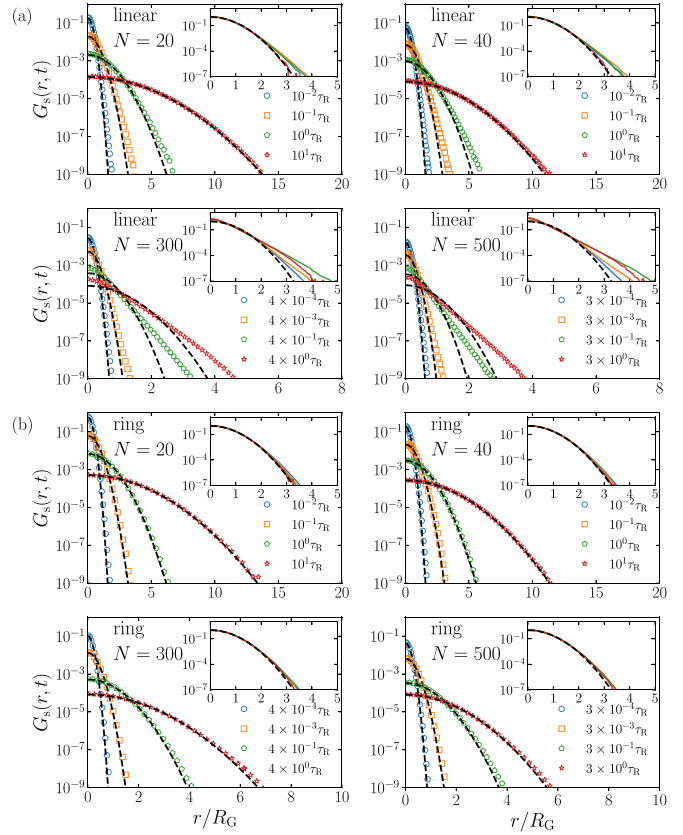


FIG. 2. Spatial correlations of the self-correlation function  $G_s(r, t)$  for linear (a) and ring (b) polymer melts of different degrees of polymerization  $N$ . Symbols: MD simulations. Dashed lines: Gaussian function  $[3/(2\pi g_1)]^{3/2} \exp[-3r^2/(2g_1)]$ . Inset: normalized curves of the  $G_s(r, t)$  with  $x$  and  $y$  axes being  $r/\sqrt{g_1}$  and  $G_s(r, t)/[3/(2\pi g_1)]^{3/2}$ , respectively.

Since the behavior of mean-squared displacements of linear and ring polymers in coarse-grained molecular dynamics simulations has been described at length by Kremer and coworkers [14,18,57], we shall not repeat such an analysis. Overall, good agreement is found between our results and those of the previous investigations.

The average non-Gaussian parameters  $\alpha_2(t)$  associated with the polymer segments are displayed in Fig. 3(c). All the ring polymers have nearly zero  $\alpha_2(t)$  in the entire observed correlation time range, in accordance with the largely Gaussian function form of  $G_s(r, t)$  function in Fig. 2(b). In comparison, the  $\alpha_2(t)$  of the linear polymers increases with chain length: the maximum value of  $\alpha_2(t)$  starts from  $\alpha_2(t) \approx 0.1$  in  $N = 20$  and reaches  $\alpha_2(t) \approx 0.5$  in  $N = 500$ . The  $\alpha_2(t)$  values of the long linear entangled polymers are comparable to the one observed in glassy polymers, which is around  $\alpha_2(t) = 0.4$  [23]. Most interestingly, all the non-Gaussian parameters  $\alpha_2(t)$  of the linear chains approach a maximum around the Rouse relaxation time  $\tau_R$ .

The average non-Gaussian parameters  $\alpha_2(t)$  for the center-of-mass self-motions are presented in Fig. 3(d). Similar to the results in Fig. 3(c), the center of mass of ring polymer exhibits essentially Gaussian behavior, with  $\alpha_2(t) \approx 0$ . For the linear chains, the non-Gaussianity of c.m. motions is insignificant

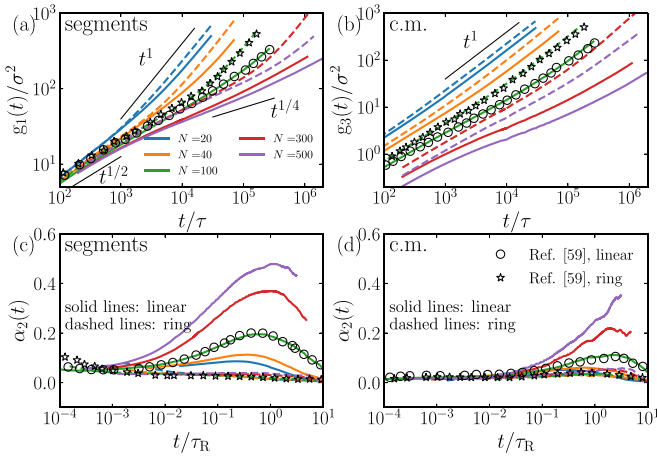


FIG. 3. Mean-square displacements (a)  $g_1(t)$  (total) and (b)  $g_3(t)$  (center of mass). (c) Average non-Gaussian parameter  $\alpha_2(t)$  for self-motions of all the segments. (d) Average non-Gaussian parameter  $\alpha_2(t)$  for the center of mass (c.m.). Solid lines: linear polymers. Dashed lines: ring polymers. Circles: results from Ref. [59] for the  $N = 100$  linear chain. Pentagrams: results from Ref. [59] for the  $N = 100$  ring. Note that the peak associated with the  $\alpha$  relaxation falls outside the time window of panel (c). The peak in  $\alpha_2(t)$  for  $\alpha$  relaxation is displayed in Fig. 9.

for the short unentangled melts, but becomes substantial in the entangled systems. Additionally, the maximum of c.m.  $\alpha_2(t)$  appears at correlation times longer than the Rouse relaxation time  $\tau_R$ . In the case of  $N = 300$  and  $N = 500$ , the  $\alpha_2(t)$  keeps increasing up to  $\sim 9\tau_R$  and does not reach a maximum within our simulation time.

The non-Gaussian behavior observed in the average self-dynamics [Figs. 3(c) and 3(d)] are consistent with a recent simulation work [59], where the authors also found significantly reduced non-Gaussian parameter  $\alpha_2(t)$  in ring polymers. To reconcile such a result with the previous NSE experiments on unentangled rings [36], it was suggested [59] that potential contamination by linear chains might have played a role in the experimental observation. In Sec. IV we discuss a few additional issues that could affect the interpretation of the NSE data. A definitive reconciliation of the experimental and simulation results on the ring polymers is beyond the scope of this work. Nevertheless, as shall be shown in the following subsections with the two-step analysis, the cyclic symmetry of a ring polymer does eliminate an important contributing factor to the non-Gaussian behavior of the average self-dynamics.

## B. Two-step analysis

Having reviewed the general features of the *average* self-dynamics of linear and ring polymers from coarse-grained molecular dynamics simulations (at temperatures far above the glass transition), we now turn to the proposed “two-step” analysis to seek a deeper understanding of the observed non-Gaussian behavior in linear chains and the largely Gaussian behavior in rings. Additionally, the appearance of a maximum in  $\alpha_2(t)$  around the Rouse relaxation time  $\tau_R$  [Fig. 3(c)] also begs an explanation. To this end, the segment dependent self-

correlation function  $G_s(\mathbf{r}, t; i)$ , mean-squared displacement  $g_1(t; i)$ , and non-Gaussian parameter  $\alpha_2(t; i)$  are computed for each segment and shown in Figs. 4 and 5. In the preceding discussion of theoretical models, two sources of non-Gaussian behavior have been identified from a mathematical point of view. (A more in-depth analysis of theoretical models will be given in the next subsection.) On the one hand, the variation of self-correlation function  $G_s(\mathbf{r}, t; i)$  along the chain can give rise to non-Gaussian behavior of the average self-correlation function  $G_s(\mathbf{r}, t)$ , even if the  $G_s(\mathbf{r}, t; i)$  of each segment is completely Gaussian (e.g.,  $\alpha_2(t; i) = 0$  as in the Rouse model). On the other hand, entanglement constraints are expected to produce non-Gaussian behavior for  $G_s(\mathbf{r}, t; i)$  (e.g., the tube model). A proper understanding of the average self-correlation  $G_s(\mathbf{r}, t)$  thus requires a two-step analysis, where  $G_s(\mathbf{r}, t; i)$  serves as a central quantity.

Figure 4 indicates that both aforementioned factors contribute to the *average* non-Gaussian behavior of linear chains. On timescales shorter than the terminal relaxation time ( $\tau_R$  for unentangled polymers and  $\tau_d$  for entangled polymers), the non-Gaussian parameter  $\alpha_2(t; i)$  is positive on the segment level for all the chain lengths. At a given correlation time,  $\alpha_2(t; i)$  increases with increase of chain length (Fig. 4), consistent with the behavior of the average  $\alpha_2(t)$ . To illustrate the variation of segment displacement along the chain, the normalized mean-squared displacement  $g_1(t; i)/g_1(t)$  is shown in Fig. 4. Similar to the predictions of Rouse-like equations [Eqs. (11) and (15)], higher relative mobility is found for the chain ends. Here four details are worth noting. First, for each chain length, the maximum of the average non-Gaussian parameter  $\alpha_2(t)$  is larger than that of the segment  $\alpha_2(t; i)$ . This implies that the variation of segment self-dynamics  $G_s(\mathbf{r}, t; i)$  along the chain is an important contributor to the average non-Gaussian behavior. A further numerical demonstration of the intrachain averaging effect on  $\alpha_2(t)$  will be given in Fig. 6 below. Second, the largest ratio of  $g_1(t; i)/g_1(t)$  predicted by Eqs. (11) and (15) is approximately 1.8. However, much higher values ( $g_1(t; i)/g_1(t) \approx 3$ ) are observed in entangled linear polymers (Fig. 4). This is probably due to a lack of consideration of both local and contour length fluctuations in the derivation of Eq. (15). Third, the non-Gaussian parameter  $\alpha_2(t; i)$  increases dramatically beyond the correlation time of  $\tau_e$  in the long chains, suggesting that the entanglement phenomenon enhances “local heterogeneity” in polymer self-dynamics. This result can be understood as follows: on the one hand, the entanglement constraints make the segmental displacements parallel and perpendicular to the primitive paths drastically different; on the other hand, the spatial fluctuations of entanglements also broadens the distribution of displacement for a given segment  $i$ . Therefore, the self-correlation function  $G_s(\mathbf{r}, t; i)$  becomes strongly non-Gaussian at  $t > \tau_e$  in entangled systems. Lastly, Fig. 4 reveals that the non-Gaussian parameter for each segment  $\alpha_2(t; i)$  does not reach a maximum at  $\tau_R$  for the entangled chains. The appearance of a maximum in the average  $\alpha_2(t)$  around  $\tau_R$  (Fig. 3) should thus be mainly attributed to the intrachain averaging of the segment self-correlation function  $G_s(\mathbf{r}, t; i)$  [Eq. (6)].

In the special case of ring polymers, the intramolecular averaging process of segment self-correlation  $G_s(\mathbf{r}, t; i)$  [Eq. (6)] no longer contributes to the average non-Gaussian

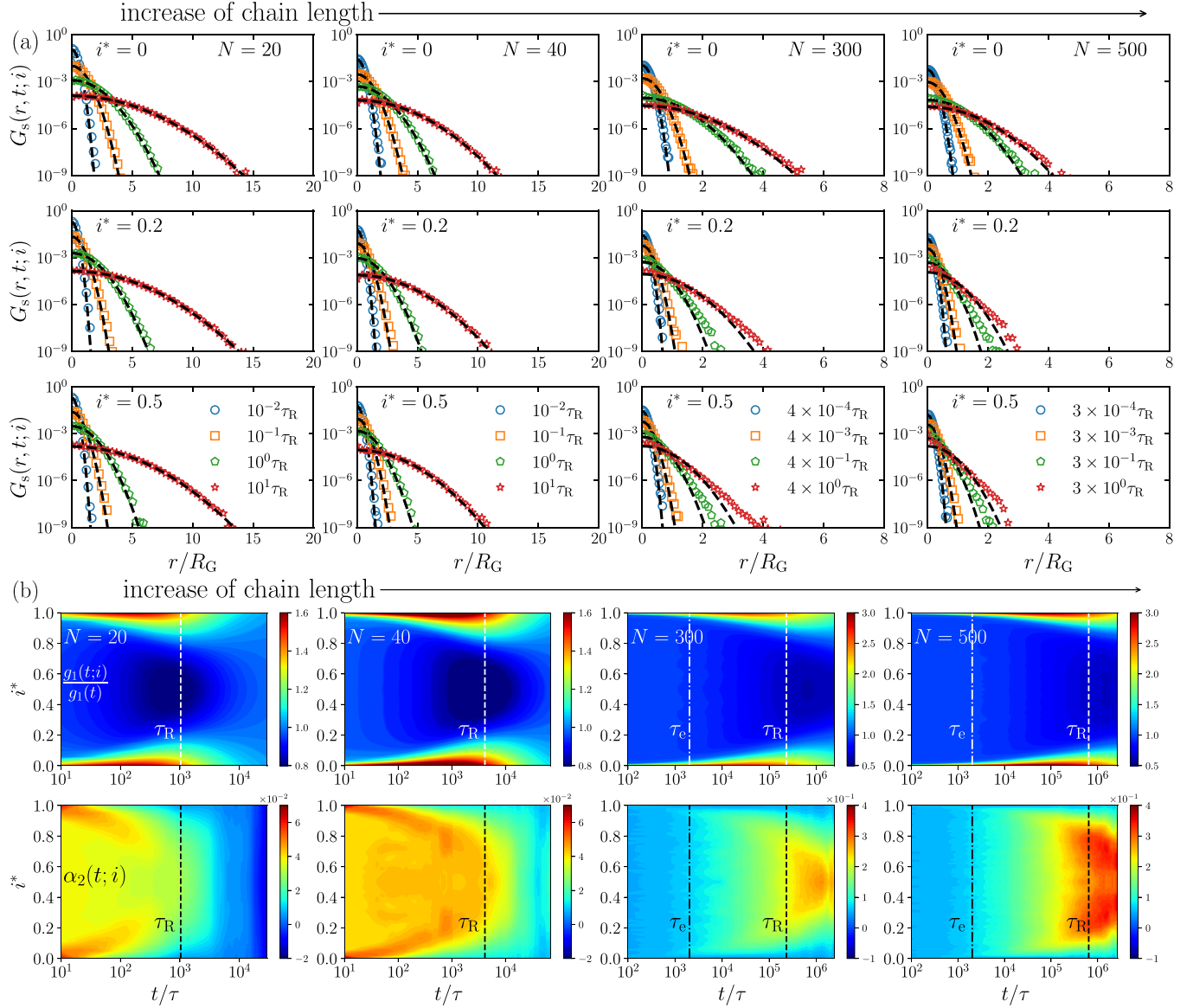


FIG. 4. Two-step analysis of self-dynamics for linear chains. (a) Self-correlation functions  $G_s(r, t; i)$  of different segments ( $i^* = 0, 0.2$ , and  $0.5$ ) at different degrees of polymerization  $N$  ( $N = 20, 40, 300$ , and  $500$ ). Dashed lines: Gaussian reference curves. (b) Full two-dimensional temporal maps of  $g_1(t; i)/g_1(t)$  and  $\alpha_2(t; i)$  for different chain lengths. Note that different color bars are used for different chain lengths.

behavior, due to the cyclic symmetry of the molecule (i.e., all the segments are identical). Not surprisingly,  $g_1(t; i)$  and  $\alpha_2(t; i)$  of the rings show no dependence on the segment index  $i$  (Fig. 5), indicating  $g_1(t) = g_1(t; i)$  and  $\alpha_2(t) = \alpha_2(t; i)$  as expected. In contrast to the behavior of linear chains, the non-Gaussian parameter for each segment  $\alpha_2(t; i)$  (“local heterogeneity”) remains small up to  $N = 500$ . We note that the concept of entanglement is controversial and poorly understood for ring polymers. According to the estimated entanglement spacing  $N_{e, \text{ring}}$  from a previous coarse-grained molecular dynamics investigation [57], the  $N = 300$  and  $N = 500$  rings in our study should be slightly entangled. However, the strong non-Gaussian behavior associated with entanglement constraints is not observed. This finding suggests that the nature of entanglement is different in rings—a conclusion that has also been reached from analysis of other dynamic properties [57]. As suggested in Ref. [60], a systematical in-

vestigation of collective dynamics through probability density functions in both real and reciprocal spaces might be helpful for understanding the difference between entanglements in linear and ring polymers. Although cooperative motions of polymer chains are beyond the scope of the current work, they can be a fruitful area of research in the future.

### C. Comparison with theoretical models

The preceding discussions have briefly touched upon the predictions of the Rouse and tube models. A more in-depth analysis of these two models will be given based on the two-step approach in this subsection. The slip-spring model [61], which is capable of providing a reasonable description of the self-dynamics of entangled polymers [17,19], will also be discussed. The main purpose of the current analysis is not to critically examine any theories of polymer dynamics,

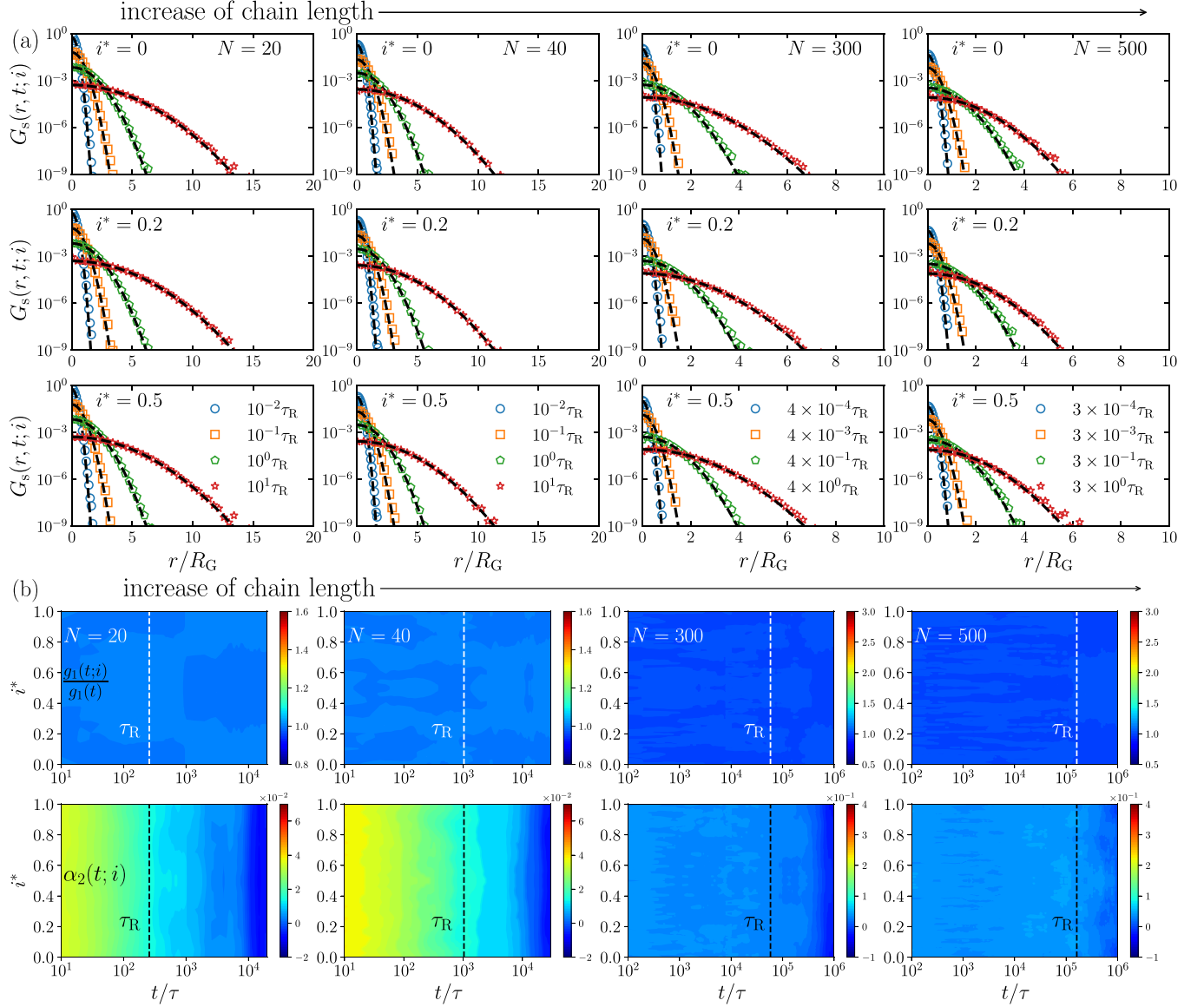


FIG. 5. Two-step analysis of self-dynamics for rings. (a) Self-correlation functions  $G_s(\mathbf{r}, t; i)$  of different segments ( $i^* = 0, 0.2$ , and  $0.5$ ) at different degrees of polymerization  $N$  ( $N = 20, 40, 300$ , and  $500$ ). Dashed lines: Gaussian reference curves. (b) Full two-dimensional temporal maps of  $g_1(t; i)/g_1(t)$  and  $\alpha_2(t; i)$  for different degrees of polymerization  $N$ .

but to benchmark the segment dependent self-dynamics [e.g.,  $G_s(\mathbf{r}, t; i)$ ] from the coarse-grained MD simulations against three useful models in the literature.

### 1. Rouse model

The Rouse model predicts that the self-correlation function  $G_s(\mathbf{r}, t)$  of a linear chain is *slightly non-Gaussian* due to the variation of  $G_s(\mathbf{r}, t; i)$  with the segment index  $i$ . By contrast, such an effect is completely absent in rings as a result of their cyclic symmetry. Quantitatively, the  $g_1(t; i)$  of a Rouse ring polymer is [4,62]

$$g_{1,\text{ring}}(t; i) = 6D_G t + \frac{4Nb^2}{\pi^2} \times \sum_{p:\text{even}} \frac{1}{p^2} \{1 - \exp[-tp^2/(4\tau_{R,\text{ring}})]\}. \quad (17)$$

Unlike Eq. (11), the dependence of  $g_1(t; i)$  on  $i$  vanishes in Eq. (17), and the self-correlation function  $G_s(\mathbf{r}, t)$  is given by

$$G_s(\mathbf{r}, t) = \left( \frac{3}{2\pi g_{1,\text{ring}}(t)} \right)^{3/2} \exp\left( -\frac{3\mathbf{r}^2}{2g_{1,\text{ring}}(t)} \right), \quad (18)$$

which is *strictly Gaussian* according to the Rouse model.

Figure 6 shows the predictions of the Rouse model for linear and ring polymers, obtained from Brownian dynamics simulations. A reduced time  $t^* = t/\tau_0$  is used to present the Brownian dynamics data, where  $\tau_0 = \zeta b^2/2k_B T$ ,  $\zeta$  is the friction coefficient, and  $b$  the segment size (see Appendix A for details). In principle, the same results can be computed by using the analytical expressions [Eqs. (11) and (13) for linear chains and Eqs. (18) and (17) for rings]. Nevertheless, we employed BD simulations as a direct check of the dynamic Gaussian approximation. Not surprisingly,



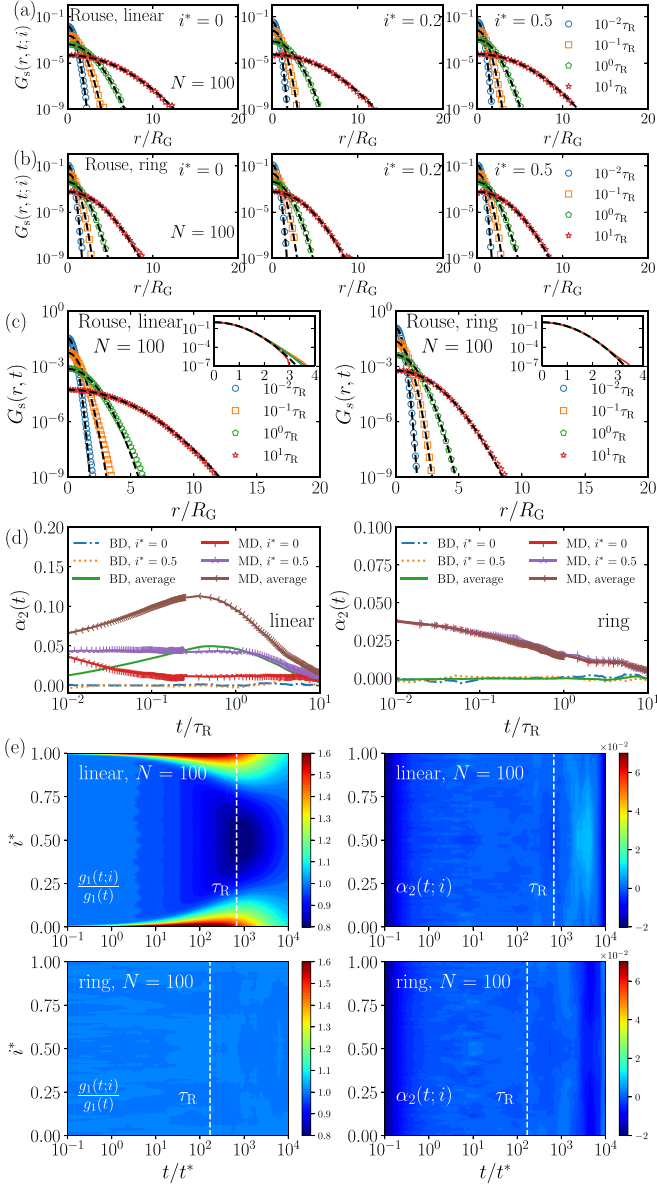


FIG. 6. Real-space self-dynamics predicted by the Rouse model for linear and ring polymers of  $N = 100$ . (a, b) Self-correlation functions of different segments  $G_s(r, t; i)$  for linear (a) and ring (b) polymers, respectively. (c) Self-correlation functions  $G_s(r, t)$  at different correlation times. Symbols in panels (a)–(c) represent the Rouse model. The dashed lines are reference Gaussian functions. The inset in panel (c) displays the normalized self-correlation function presented in the same way as Fig. 2. (d) Comparison of the non-Gaussian parameters of different segments  $\alpha_2(t; i)$  and the averaged value of all the beads  $\alpha_2(t)$ . MD: results from linear and ring polymers with  $N = 40$ . (e) Two-dimensional temporal maps of  $g_1(t; i)/g_1(t)$  and  $\alpha_2(t; i)$ . The vertical dashed lines indicate the Rouse relaxation time.

good agreement has been found between the analytical and numerical solutions. According to the Rouse model, the self-correlation function  $G_s(\mathbf{r}, t; i)$  is Gaussian for every segment  $i$ , regardless of the chain architecture [Figs. 6(a) and 6(b)]. However, the average self-correlation function  $G_s(\mathbf{r}, t)$  for all the segments is slightly non-Gaussian for the linear chain, in

contrast to the behavior of the ring [Fig. 6(c)]. As explained in Sec. II, the non-Gaussianity of the linear chain comes from the variation of self-dynamics with the segment index  $i$ : the arithmetic average of Gaussian functions with distinct variances is non-Gaussian. This issue is further illustrated in Fig. 6(d), where the results of MD simulations of linear and ring polymers with  $N = 40$  are also added as a comparison. As noted in the preceding discussion,  $\alpha_2(t)$  is generally not an arithmetic average of  $\alpha_2(t; i)$  of individual segments. For the Rouse model, the average  $\alpha_2(t)$  is nonzero over a wide range of timescales and displays a peak around  $\tau_R$  [Fig. 6(d)], while the non-Gaussian parameters  $\alpha_2(t; i)$  of  $i^* = 0$  and 0.5 remain zero throughout. This behavior is due to the dependence of mean-squared displacement  $g_1(t; i)$  (variance of  $G_s(\mathbf{r}, t; i)$ ) on the segment position (index)  $i$ , which can be visualized by presenting  $g_1(t; i)/g_1(t)$  as a two-dimensional map [Fig. 6(e)].

Several useful conclusions can be reached from the comparison of the MD simulations and the Rouse model predictions for unentangled polymers [Figs. 3–6]. First, the Rouse model qualitatively captures the variation of mean-squared displacement  $g_1(t; i)$  along the chain: the chain ends are much more mobile than the middle portion of the chain on intermediate timescales. It should be noted, however, that such a “chain-end effect” on polymer slow dynamics is fundamentally different from the one observed on short timescales for polymer  $\alpha$  relaxation (see Sec. III D for details). Second, the Rouse model fails to conceive the non-Gaussian behavior of  $G_s(\mathbf{r}, t; i)$ . To our knowledge, the peculiar segment dependence of  $\alpha_2(t; i)$  observed in the MD simulations is not predicted by any existing theories. The previous discussions of the failure of the Rouse model [33,34] placed emphasis on the c.m. motions. The current analysis provides additional information about the non-Gaussian behavior of unentangled polymer melts. Third, similar to the case of the Rouse model, intrachain averaging of distinct self-correlation functions  $G_s(\mathbf{r}, t; i)$  is a significant contributing factor to the overall non-Gaussian behavior. The average  $\alpha_2(t)$  from the MD simulations is not only much higher than the  $\alpha_2(t; i)$  of individual segment  $i$ , but also has rather different time dependence [Fig. 6(d)].

## 2. Tube model

The segment self-intermediate scattering function  $F_s(\mathbf{Q}, t; i)$  of the tube model [Eq. (14)] was first given in the seminal 1978 paper of Doi and Edwards [48] and later reiterated in their classical monograph on polymer dynamics [4]. Surprisingly, this prediction has not been thoroughly examined against any molecular simulations. Computational studies in the past primarily focused on various average mean-squared displacements [i.e., the so-called  $g_1(t)$ ,  $g_2(t)$ , and  $g_3(t)$ ] [14,18], which is merely one aspect of polymer self-dynamics [63]. An in-depth analysis of the real-space self-dynamics of the classical tube model is thus necessary. A discussion of an approximate formula for the average self-intermediate scattering function  $F_s(\mathbf{Q}, t)$  and the corresponding self-correlation function  $G_s(\mathbf{r}, t)$  is given in Appendix C.

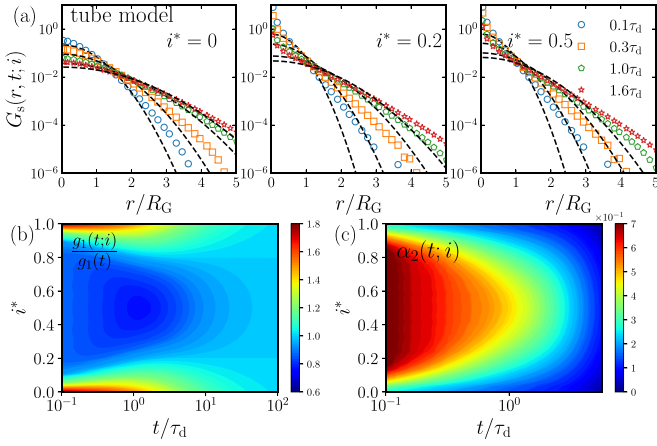


FIG. 7. Real-space self-dynamics of entangled polymers predicted by the tube model. (a) Self-correlation functions of different segments  $G_s(r, t; i)$  according to the tube model. Dashed lines: Gaussian reference curves. (b) Variation of segment mean-squared displacement  $g_1(t; i)/g_1(t)$  along the chain. (c) Variation of the non-Gaussian parameter  $\alpha_2(t; i)$  along the chain.

Equation (14) can be straightforwardly evaluated by numerically finding the solutions of the equations  $\alpha_p \tan \alpha_p = \mu$  and  $\beta_p \cot \beta_p = -\mu$ . The real-space self-correlation function  $G_s(r, t; i)$  is then computed through Hankel transform of  $F_s(Q, t; i)$ . The mean-squared displacement  $g_1(t; i)$  can be obtained from the integral  $g_1(t; i) = \int \mathbf{r}^2 G_s(\mathbf{r}, t; i) d\mathbf{r}$  or directly from Eq. (15). The non-Gaussian parameter  $\alpha_2(t; i)$  for each segment is evaluated from the self-correlation function  $G_s(r, t; i)$  using Eq. (10).

Figure 7 presents the results of our calculations, where the reptation time  $\tau_d = 3Z\tau_R$  is used as a time unit, with  $Z$  being the number of entanglements per chain. Regardless of the segment index  $i^*$ , the segment self-correlation function  $G_s(r, t; i)$  exhibits strong non-Gaussian behavior. In the middle portion of the chain, where  $G_s(\mathbf{r}, t; i) \approx G_s(\mathbf{r}, t)$ , the self-correlation function resembles a Dirac- $\delta$  function at small distances as a result of tube confinement and develops an exponential-like tail at large distances. Strictly speaking, the prediction of the tube model is only valid at long correlation time  $t \gg \tau_R$ —a timescale that is difficult to investigate with simulations of the coarse-grained bead-spring model. Nevertheless, the MD simulation results can still be useful for checking the theoretical predictions in a qualitative way. Our MD simulations show that the self-correlation function does not display any significantly enhanced distribution at  $r \approx 0$ . Although the classical tube model envisions variations of mean-squared displacement  $g_1(t; i)$  along the chain, Eqs. (14) and (15) do not give quantitatively correct results, due to the lack of a proper consideration of local and contour length fluctuations in the derivation. The largest ratio of  $g_1(t; i)/g_1(t)$  predicted by Eq. (15) is approximately 1.8, while the difference can be as large as 3.0 in the molecular dynamics simulations. Lastly, the “strong” tube confinement effect in this version of the model leads to large non-Gaussian parameters  $\alpha_2(t; i) \approx 0.7$ . By contrast, the highest value of  $\alpha_2(t; i)$  is approximately 0.4 in the simulations of the  $N = 500$  chain.

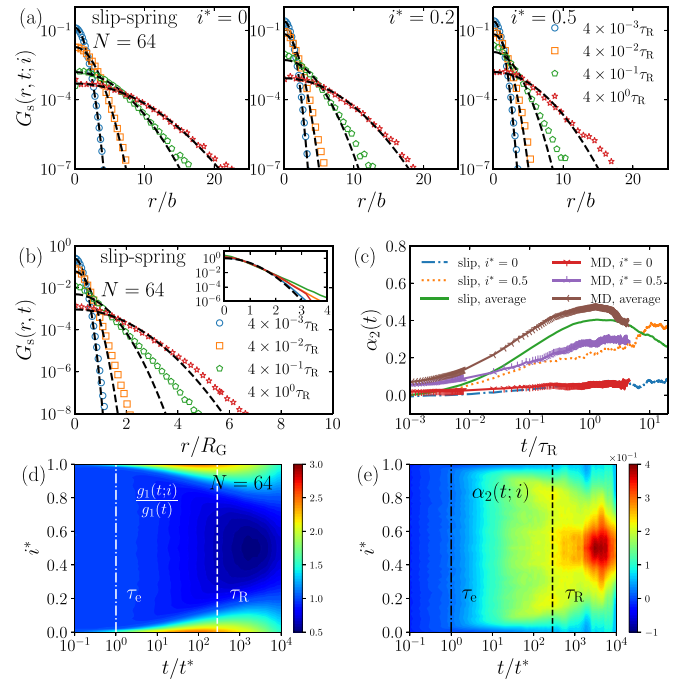


FIG. 8. Simulation results of the slip-spring model for  $N = 64$ . (a) Self-correlation functions of different segments  $G_s(r, t; i)$  according to the slip-spring model. (b) Self-correlation function  $G_s(r, t)$  at different correlation times. Dashed lines: Gaussian functions. (c) Comparison of the non-Gaussian parameters of different segments  $\alpha_2(t; i)$  and the averaged values from all segments along a polymer chain  $\alpha_2(t)$ . MD: results for the linear chain of length  $N = 500$  from the MD simulations. (d, e) Two-dimensional temporal maps of  $g_1(t; i)/g_1(t)$  and  $\alpha_2(t; i)$ .

### 3. Slip-spring model

The slip-spring model of Likhtman [61] overcomes several of the aforementioned artifacts of the original tube model [48], by using “soft” entanglement confinement and introducing constraint release. Unlike a few other notable slip-link models [64–66], the slip-spring model considers fluctuations on small time and length scales and therefore can be directly compared with coarse-grained molecular dynamics simulation and neutron spin-echo experiments [19,61]. Our previous investigation [19] showed that the slip-spring model provides a reasonable description of the self-dynamics of entangled polymers in the reciprocal space. In this work, we extend the analysis to the real space. Note that the entanglement equilibration time in this slip-spring model is  $\tau_e \approx t^*$ . The results of the slip-spring simulations are displayed in Fig. 8. Both the exponential tail in  $G_s(r, t)$  and the maximum  $\alpha_2(t)$  values of the slip-spring model are comparable to those of the linear entangled systems in the MD simulations. The artificial enhancements of both  $G_s(r, t; i)$  and  $G_s(r, t)$  at  $r \approx 0$  are also removed [Figs. 8(a) and 8(b)]. Interestingly, the average non-Gaussian parameter  $\alpha_2(t)$  shows a maximum around  $\tau_R$  while the  $\alpha_2(t; i)$  of individual segment reaches a maximum at a much later correlation time. This observation is in broad agreement with the MD simulations and can be understood as a result of the intramolecular averaging process of self-dynamics. In addition, the constraint release effect on the

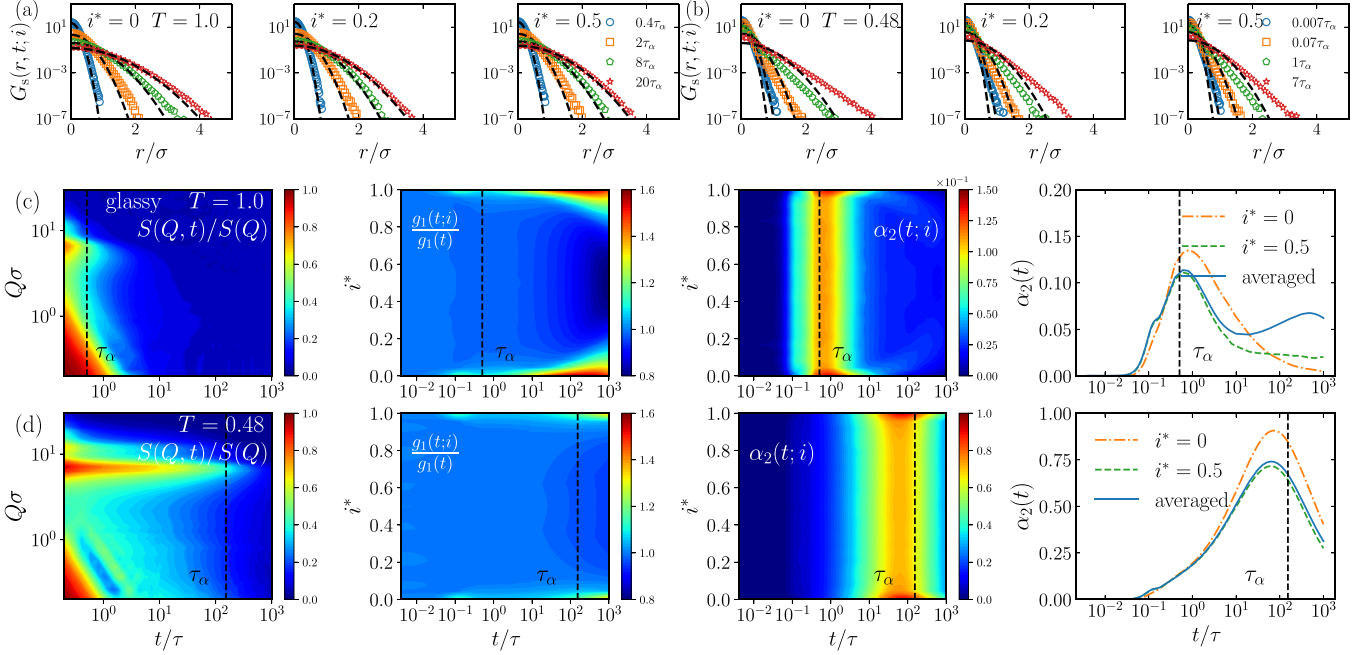


FIG. 9. Application of the two-step analysis to polymer  $\alpha$  relaxation (“glassy dynamics”). (a, b) Self-correlation functions of different segments  $G_s(r, t; i)$  at (a)  $T = 1.0$  and (b)  $T = 0.48$ . (c, d) Other dynamical information. First column: spatiotemporal maps of normalized coherent intermediate scattering function  $S(Q, t)/S(Q)$ . Second column: variation of segment mean-squared displacement  $g_1(t; i)/g_1(t)$  along the chain. Third column: variation of non-Gaussian parameter  $\alpha_2(t; i)$  along the chain. Fourth column: comparison of the non-Gaussian parameter of different segments and the average non-Gaussian parameter of all the beads. Vertical black dashed line:  $\alpha$  relaxation time determined from the density fluctuations at the first structural peak.

chain ends brings  $g_1(t; i)/g_1(t)$  close to the value found in the MD simulations. Lastly, the soft nature of the entanglement constraints in the slip-spring model also yields more reasonable values of  $\alpha_2(t; i)$  on the segment level. It is worth noting that similar to the case of unentangled melts [Fig. 6(d)] the average non-Gaussian parameter  $\alpha_2(t)$  behaves rather differently than the  $\alpha_2(t; i)$  of individual segments in entangled polymers as well [Fig. 8(c)]. A full understanding of the non-Gaussian self-dynamics in polymers therefore demands the knowledge of segment dependent self-correlation function  $G_s(\mathbf{r}, t; i)$ , in addition to the commonly computed average quantity  $G_s(\mathbf{r}, t)$ .

#### D. Application to glassy dynamics

Having examined polymer melt self-dynamics from the viewpoint of two-step analysis, we now briefly discuss the application of this method to glassy dynamics. In the current context, glassy dynamics broadly refers to molecular motions related to polymer  $\alpha$  relaxation, which occur on relatively short timescales and small length scales [67]. The effects of chain ends (molecular weight) on the polymer glass transition temperature [55,56] and  $\alpha$  relaxation [68–70] have long been recognized. Since the glassy dynamics of chain ends are expected to be different from those of the middle segments, a careful consideration of self-motions at both the individual segment and chain levels appears necessary.

To pursue this idea, a coarse-grained polymer melt of chain length  $N = 25$  was investigated at  $T = 1.0$  and 0.48. The details of the simulation can be found in Appendix A.

To illustrate the overall dynamic features of this system, the collective density fluctuations  $S(Q, t)/S(Q)$  are spatiotemporally mapped out [67] over a wide range of correlation times and wave numbers and presented in Fig. 9 (first column). The  $\alpha$  relaxation time  $\tau_\alpha$  is estimated as the time when  $S(Q, t)/S(Q) = e^{-1}$  at the first structural peak of  $S(Q)$ . At high temperature ( $T = 1.0$ ), the  $\alpha$  relaxation, which can be probed by examining the density fluctuations around the first structural peak, is relatively fast ( $\tau_\alpha \approx 0.5\tau$ ). On the other hand, the relaxation behavior at the mesoscopic scale is dominated by hydrodynamic-like fluctuations [67]. When the temperature is lowered to  $T = 0.48$ , the  $\alpha$  relaxation becomes significantly slower ( $\tau_\alpha \approx 154\tau$ ) and excess density correlation develops at the mesoscopic scale. (A detailed discussion of mesoscopic collective dynamics can be found in Ref. [67].) To survey the heterogeneity of self-dynamics, segment dependent self-correlation function  $G_s(r, t; i)$ , the relative segment mean-squared displacement  $g_1(t; i)/g_1(t)$ , and non-Gaussian parameter  $\alpha_2(t; i)$  are computed and shown as a function of the normalized segment index  $i^*$  and correlation time  $t$  in Fig. 9. Interestingly, the features revealed by these analyses are distinctly different from those of Rouse and reptation dynamics. First, while the chain ends are indeed more mobile than the middle segments, with higher mean-squared displacements  $g_1(t; i)$ , such a difference diminishes rapidly as the segment index moves towards the center. By contrast, the variation of mean-squared displacement  $g_1(t; i)$  is controlled by Rouse-like dynamics [Eqs. (11) and (15)] and penetrates much deeper into the “interior” of the chain (e.g., Figs. 4, 6–8). Second, the self-dynamics of chain ends around  $\tau_\alpha$  are

substantially more non-Gaussian than those of the middle segments [Figs. 9(a)–9(c), third column]. A completely opposite trend is observed for slow dynamics (Figs. 4, 7, and 8).

It should be noted that short chains are commonly used in coarse-grained simulations of polymer glassy dynamics [50,71–76], with a typical chain length  $N$  in the neighborhood of 10–20 beads. In these cases, the average self-correlation  $G_s(\mathbf{r}, t)$  as well as the non-Gaussian parameter  $\alpha_2(t)$  should be strongly influenced by the contributions from the chain ends [e.g., Fig. 9(c), fourth column]. In principle, this problem can be alleviated using long chains. However, such a solution is far from a prevailing practice, nor can it always be implemented in a straightforward manner for low-temperature simulations.

Additionally, the difference between the non-Gaussian parameters of chain ends and middle segments presents some interesting questions and perhaps also clues about the nature of heterogeneity in polymer glassy dynamics. A few *speculative* comments are thus provided below. First, for density fluctuations on short timescales (e.g.,  $\alpha$  relaxation), the local packing environment must lie at the root of the elevated non-Gaussian parameter of the chain ends compared to the middle segments. For slow dynamics, the difference in the local environment is averaged out and becomes unimportant, and entanglements appear to be the main driving force of non-Gaussian self-dynamics (Fig. 3). According to the classical tube picture [10,48], on timescales shorter than the reptation time, the central segments are still strongly confined in the original tube, while the chain ends can move freely to explore new tube segments, leading to enhanced non-Gaussian behavior at the center of the chain (Figs. 7 and 8). Second, in studies of glass-forming liquids, the structural relaxation ( $\alpha$  relaxation) is often characterized by two parameters: fragility [77]  $m$  and stretched exponential (Kohlrausch-Williams-Watts) exponent  $\beta$ , which are strongly correlated with each other [78]. The non-Gaussian parameter  $\alpha_2(t)$  is expected to be closely connected to the stretched exponential exponent  $\beta$  [24], although its relation to fragility is less clear. Additionally, the molecular weight dependence of fragility in polymers appears to be nonuniversal [79]. The result in Fig. 9, taken at the face value, implies that a decrease of chain end concentration (i.e., increase of molecular weight) would reduce the overall, averaged non-Gaussian behavior—a deduction that remains to be verified. Finally, the analysis given here serves mainly as an example to illustrate the importance of separating inter-chain and intrachain averaging of polymer self-dynamics. Our coarse-grained simulations at two temperatures merely reveal the tip of the iceberg and further systematic computational studies are clearly desired.

#### IV. ADDITIONAL COMMENTS ON THE RING SIMULATIONS

Our simulations of ring polymer melts have revealed largely Gaussian self-dynamics for ring polymers, which is in line with another coarse-grained MD simulation study [59] but at odds with the NSE experiments [36]. Interestingly, our analysis indicates that two important contributing factors to the average non-Gaussian parameter  $\alpha_2(t)$  are indeed suppressed or completely eliminated in ring polymers. On

the one hand, intrachain averaging of distinct segment self-correlation function  $G_s(\mathbf{r}, t; i)$  leads to significantly enhanced non-Gaussianity in the averaged self-dynamics  $G_s(\mathbf{r}, t)$  of linear chains [e.g., Figs. 6(d) and 8(c)]. But this is not an issue for rings due to their cyclic symmetry. On the other hand, we show that polymer entanglement substantially increases the non-Gaussianity of self-dynamics  $G_s(\mathbf{r}, t; i)$  at the individual segment level (Fig. 4). Such an effect is also suppressed in rings (Fig. 5), probably as a result of lack of effective entanglements [57].

In addition to the potential contamination by linear chains [59], neutron spin-echo spectroscopy [33–36] measurements of ring polymers may suffer a few other problems. In these experiments on isotopically labeled, *unentangled* polymer melts, *coherent* scattering dominates the NSE intermediate scattering function (ISF) and the normalized ISF,  $S(Q, t)/S(Q)$ , is typically analyzed in accordance to the Rouse model. For example, the prediction of the Rouse model for the single-chain dynamic structure  $S(\mathbf{Q}, t)$  of a linear chain is [4]  $S(\mathbf{Q}, t) = \frac{1}{N} \sum_{i,j} \exp\{-\mathbf{Q}^2 D_G t - \frac{1}{6}|i-j|\mathbf{Q}^2 b^2 - \frac{2N b^2 \mathbf{Q}^2}{3\pi^2} \sum_{p=1}^{\infty} \cos(\frac{p\pi i}{N}) \cos(\frac{p\pi j}{N}) [1 - \exp(-t p^2/\tau_{R,\text{linear}})]\}$ . The first term in the exponential function,  $\exp(-\mathbf{Q}^2 D_G t)$ , is the contribution of the center-of-mass diffusion, which prevails in the long-time limit. The second term yields the single-chain static structure factor in the short-time limit ( $t = 0$ ):  $S(\mathbf{Q}) = \frac{1}{N} \sum_{i,j} \exp(-\frac{1}{6}|i-j|\mathbf{Q}^2 b^2)$ . The last term is the scattering contribution from internal motions. Deviations from the Rouse model predictions were observed in previous NSE measurements of both linear and ring polymers [33,35,36]. The origin of such a failure was attributed to non-Gaussian c.m. diffusion, which is not accounted for in the Rouse model.

Our recent spatial correlation analysis [19] of unentangled and entangled polymers revealed, however, that the failure of the Rouse model to describe *coherent* polymer dynamics stems primarily from its inability to accurately capture collective internal motions. In the short-time limit, the Rouse model predicts that  $S(Q, t)/S(Q) \sim \exp[-(Q^2 \xi_t^2)^\beta / 6]$ , with  $\beta \approx 1.5$ .  $\xi_t$  is the characteristic length for the spatial decay of  $S(Q, t)/S(Q)$  at a given correlation time [19]. On the other hand, our simulations and NSE experiments indicate that the spatial correlation of the normalized single-chain dynamic structure factor  $S(Q, t)/S(Q)$  is only a slightly compressed Gaussian function with  $\beta \approx 1.1$  [19]. Therefore, a remedy of the Rouse model must go beyond simple introduction of non-Gaussian displacements of the center of mass [80]. Conversely, estimating non-Gaussian displacements from the coherent scattering function with the Rouse model formula would be indirect and inaccurate. In addition, the cumulant expansion approach [81–83] adopted in the previous NSE work on ring polymers [36] may involve further complications. First, it was assumed that the measured coherent intermediate scattering function was dominated by the center-of-mass diffusion. But this assumption was difficult to justify for a wide range of correlation times. Second, the non-Gaussian behavior generally shows up as a long tail of the intermediate scattering function [19], which cannot be resolved without accurate measurements of weak correlations. Third, precise determination of  $\alpha_2(t)$  generally requires measurements at a

large number of scattering wave numbers [19]. Analysis at a few  $Q$ s is unlikely to yield reliable results. Lastly, since the non-Gaussian effect is mainly manifest in the tail of the self-intermediate scattering function (high  $Q$ ) [19], it is not obvious if truncating the cumulant expansion at the fourth order will lead to significant errors for the estimation of  $\alpha_2(t)$ . We emphasize that a definitive resolution of the apparent discrepancy between simulations and experiments is beyond the scope of this paper. It is still possible that the strong non-Gaussian c.m. diffusion observed in the NSE experiments may indeed occur in real ring polymers, due to intermolecular forces that are not accurately captured in the coarse-grained simulations.

## V. SUMMARY

The unique nature of polymers necessitates a nuanced treatment of self-dynamics, rather than simply looking at the averaged correlations, as one typically does for atomic fluids. This work shows that studies of polymer self-dynamics are different from those of atomic fluids, and calls attention to the self-correlation functions of individual segments. The idea of the “two-step” analysis is demonstrated with coarse-grained molecular dynamics simulations of polymer melts and several theoretical models. Two key contributing factors to the non-Gaussian behavior of *average* self-dynamics at high temperatures have been identified: one is intrachain averaging of distinct segment self-correlation function  $G_s(\mathbf{r}, t; i)$  and the other is the entanglement phenomenon. They are responsible for the enhancement of non-Gaussianity in linear polymers with increasing chain length, as well as the suppression of non-Gaussianity in rings. In particular, the entanglement phenomenon enhances the non-Gaussian behavior in two ways: it exacerbates the difference in self-dynamics between chain ends and central segments and gives rise to strong non-Gaussian dynamics on the individual segment level.

Finally, the applicability of the two-step approach to polymer glassy dynamics has also been demonstrated. While past investigations of polymer self-dynamics have primarily focused on the average response, a detailed consideration of segment dependent self-correlation function  $G_s(\mathbf{r}, t; i)$  is clearly necessary from both the mathematical and physical points of view. Our proposed method should be useful for not only polymer melts, but also other types of polymeric materials, including polymer blends [84], polymer electrolytes [85,86], and polymer nanocomposites [87–90].

## ACKNOWLEDGMENTS

Z.S. and Y.W. acknowledge support by the U.S. Department of Energy (DOE), Office of Science, Office of Basic Energy Sciences, Early Career Research Program Award No. KC0402010, under Contract No. DE-AC05-00OR22725. This research was performed at the Oak Ridge National Laboratory’s Center for Nanophase Materials Sciences, which is a DOE Office of Science User Facility. Our computational investigation used resources of the Oak Ridge Leadership Computing Facility at the Oak Ridge National Laboratory, which is supported by the DOE Office of Science under Contract No. DE-AC05-00OR22725.

## APPENDIX A: SIMULATION MODELS AND METHODS

### 1. Molecular dynamics simulations

Molecular dynamics (MD) simulations were performed with the GPU-accelerated LAMMPS package [91–93]. For both linear and ring polymers, we consider a widely used coarse-grained semiflexible bead-spring model [18,57,58]. The nonbonded interactions between beads are described by a purely repulsive Lennard-Jones (LJ) potential [94]:

$$U_{\text{LJ}}(r) = \begin{cases} 4\epsilon \left[ \left( \frac{\sigma}{r} \right)^{12} - \left( \frac{\sigma}{r} \right)^6 \right] - 4\epsilon \left[ \left( \frac{\sigma}{r_c} \right)^{12} - \left( \frac{\sigma}{r_c} \right)^6 \right] & r < r_c \\ 0 & r \geq r_c \end{cases}, \quad (\text{A1})$$

where  $r$  is the distance between two beads,  $\epsilon$  represents the energy unit, and  $\sigma$  defines the bead size. As is the convention, LJ reduced units are used in the simulations. The natural timescale is  $\tau = \sigma \sqrt{m/\epsilon}$ , with  $m$  is the mass unit. The cut-off distance  $r_c$  is set at  $r_c = 2^{1/6} \sigma$  [14,57,58]. A finitely extensible nonlinear elastic (FENE) potential is used to connect two neighboring beads in a polymer:

$$U_{\text{FENE}}(r) = -\frac{1}{2} k R_0^2 \ln[1 - (r/R_0)^2], \quad (\text{A2})$$

where  $R_0 = 1.5 \sigma$  and  $k = 30 \epsilon/\sigma^2$ . Additionally, a bond-bending potential is considered:

$$U_{\text{bend}}(\theta) = k_\theta (1 + \cos \theta), \quad (\text{A3})$$

where  $\theta$  is the angle between two successive bonds and  $k_\theta = 1.5 \epsilon$ . The simulations were carried out at temperature of  $T = 1.0$  and bead number density of  $\rho = 0.85 \sigma^{-3}$ . At these conditions, the average number of beads between entanglements is  $N_e \approx 28$  for the semiflexible linear chains [18,95]. As usual, the Rouse time for a polymer with a degree of polymerization  $N$  follows the scaling relation  $\tau_{\text{R,linear}} = \tau_0 N^2$  for linear chains and  $\tau_{\text{R,ring}} = \tau_0 N^2/4$  for rings, where the elementary Rouse time  $\tau_0 \approx 2.58 \tau$  for the current model [95]. The entanglement time of linear chain can be estimated as  $\tau_e = \tau_0 N_e^2$ . Five different degrees of polymerization,  $N = 20, 40, 100, 300,$  and  $500$ , were investigated for both the linear and ring polymers. The corresponding numbers of molecules in the simulations were  $M = 5000, 5000, 2000, 700,$  and  $500$ , respectively. The equilibrated configurations of linear and ring polymers were generated with the previously reported protocols in the literature [58,96,97]. The production runs were performed in the NVE ensemble with a weak coupling to a Langevin thermostat [14] and a damping coefficient of  $0.002$ . A typical time step of  $\Delta t = 0.01 \tau$  was used in the time integration. A benchmark of the static properties of the simulated linear and ring polymers with the previous results in the literature [18,58] is provided in Fig. 10. Additionally, we note that the dynamic properties of our simulations also agree well with the previous reports (Fig. 3).

In addition, a slightly different coarse-grained semiflexible bead-spring model [67,98] was also investigated to demonstrate the applicability of the two-step approach to polymer glassy dynamics. In this model, the nonbonded interactions between beads are described by a Lennard-Jones potential with  $r_c = 2.5 \sigma$ . The bonds along the polymer backbone are maintained by the FENE potential [Eq. (A2)], with  $R_0 = 1.5 \sigma$  and  $k = 30 \epsilon/\sigma^2$ . The bending potential is of the

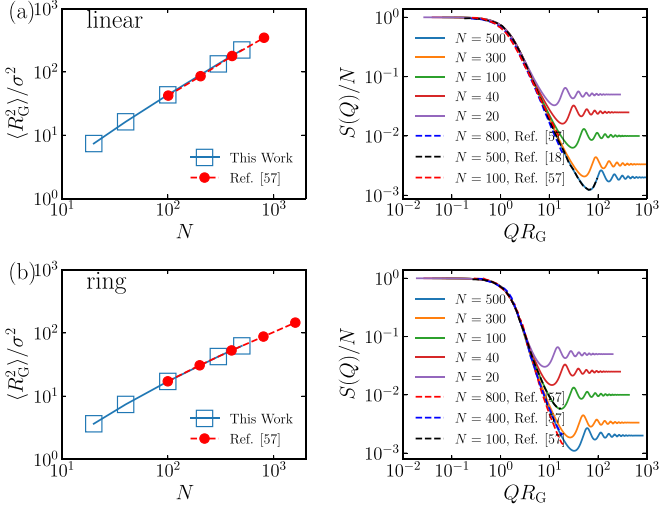


FIG. 10. Benchmark of the static properties of the (a) linear and (b) ring polymers from coarse-grained molecular dynamics simulations with the previous results in the literature [18,57]. Left column: radius of gyration  $R_G$  for polymers of different degrees of polymerization  $N$ . Right column: single-chain static structure factor  $S(Q)$ . Solid lines: current study. Dashed lines: previous reports.

same form as Eq. (A3), but slightly softer than the one used in the high-temperature melt simulations, with  $k_\theta = 0.75 \epsilon$ . An unentangled polymer melt composed of  $M = 8000$  linear chains of length  $N = 25$  was studied at two different temperatures  $T = 1.0$  and  $0.48$ . The system was first fully relaxed at  $T = 1.0$  in the NPT ensemble with  $P = 0$ . Subsequently, the temperature was gradually reduced to  $T = 0.48$  at the constant pressure with a rate of  $10^{-5}$  [54]. Before calculations of dynamic properties, the system at each temperature was further relaxed under NVT condition for more than  $5000 \tau_\alpha$ , where  $\tau_\alpha$  is the  $\alpha$  relaxation time. The final production runs were performed in the NVT ensemble. Additional details of this simulated polymeric system, including both the static and dynamic properties, can be found in our previous work [67].

## 2. Brownian dynamics simulations

To complement the MD investigations and obtain deeper insight into the real-space dynamics of polymers, Brownian dynamics simulations [99] were performed with the Rouse model [46] and the slip-spring model [61]. For the Rouse model, both linear chains and rings were considered. On the other hand, the slip-spring simulations were confined to linear chains. The simple Euler method was used for the time integration in both cases. The reduced time  $t^*$  in both the Rouse and slip-spring simulations is defined as  $t^* = t/\tau_0$ , where  $\tau_0 = \zeta b^2/2k_B T$ , with  $b$  being the segment size. The Rouse model BD simulations have been validated by benchmarking the space-time density correlation functions against the well-known analytical solutions [4].

Our choice of model parameters for the slip-spring simulations followed the work of Likhtman [61]. The average entanglement spacing  $N_e$  was 4 and the spring strength  $N_s$  was  $1/2$ . The ratio  $\xi_s \equiv \zeta_s/\zeta$  of the friction coefficient of the slip

link  $\zeta_s$  to that of the chain segment  $\zeta$  was 0.1. To simplify the simulation, the noncrossing condition was not implemented for the slip links. Such a choice makes only a very small difference in the results [61]. The results presented in this work are based on the simulations with  $N = 64$  [100]. The details of the slip-spring model are described in the original paper of Likhtman [61]. Additionally, reciprocal-space correlation analysis of the slip-spring model can be found in our previous study [19].

## APPENDIX B: SELF-INTERMEDIATE SCATTERING FUNCTION OF THE ROUSE MODEL

The self-intermediate scattering function  $F_s(\mathbf{Q}, t)$  [Eqs. (11) and (12)] of a linear Rouse chain is well documented in the literature [4]. The spatial correlation of the Rouse model  $F_s(\mathbf{Q}, t)$ , *strictly speaking*, is non-Gaussian, as discussed and demonstrated numerically in the main text. An approximation of Eqs. (11) and (12) is [4,101]

$$F_s(\mathbf{Q}, t) \approx \exp\left(-\frac{2}{\pi^2} \tilde{\mathbf{Q}}^2 \tilde{t}\right) \exp\left(-\frac{2}{\pi^{3/2}} \tilde{\mathbf{Q}}^2 \tilde{t}^{1/2}\right), \quad (\text{B1})$$

with  $\tilde{\mathbf{Q}} = \mathbf{Q}R_G$  and  $\tilde{t} = t/\tau_R$ . The first exponential function describes the contribution from the center-of-mass diffusion, which is unimportant for  $t \ll \tau_R$ ; the second exponential function comes from internal motions. This formula is obtained by making the approximation

$$F_s(\mathbf{Q}, t) \approx \exp\left(-\frac{1}{6} \mathbf{Q}^2 g_1(t)\right), \quad (\text{B2})$$

instead of performing an intrachain averaging of the self-intermediate scattering function  $F_s(\mathbf{Q}, t; i)$  of each segment according to Eq. (12). By the nature of this approximation, Eq. (B1) gives *Gaussian* spatial correlations of self-dynamics at a given correlation time, which is different from the precise analytical result [Eq. (12)]. Nevertheless, since the non-Gaussian behavior of unentangled polymers is relatively weak, the Gaussian formulas [Eqs. (B1) and (B2)] can often adequately describe their self-dynamics [7,19,41].

## APPENDIX C: REAL-SPACE SIGNATURE OF TUBE CONFINEMENT

Direct microscopic observation of tube confinement in entangled polymers has been a long-sought goal of polymer physicists. According to the classical tube theory [48,49], the self-intermediate scattering function of a reptating chain can be described by a scaled complementary error function on the timescale  $\tau_R < t < \tau_d$ :

$$F_s(\mathbf{Q}, t) \approx \exp(\mathbf{Q}^4 a^2 D t / 36) \text{erfc}(\mathbf{Q}^2 a \sqrt{D t} / 6), \quad (\text{C1})$$

where  $a$  is the tube diameter and  $D$  the curvilinear diffusion coefficient. It is helpful to note that the discussion of the self-intermediate scattering function  $F_s(\mathbf{Q}, t)$  in the Doi-Edwards paper [48] contained several typos [Eqs. (4.44), (4.45), and (4.46)]. Once these errors are corrected, the final result [Eq. (C1)] is consistent with that of Fatkullin and Kimmich [49], which was derived using a different approach. A

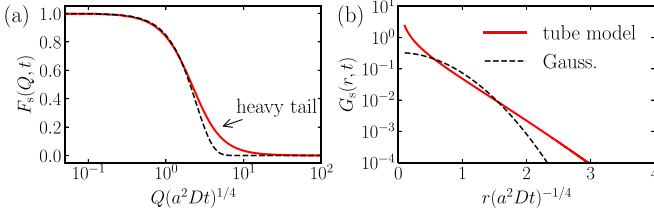


FIG. 11. (a) Spatial correlations of the average self-intermediate scattering functions  $F_s(\mathbf{Q}, t)$  predicted by the tube model [Eq. (C1)] (red solid line) and a Gaussian function (black dashed line), where  $F_s(\mathbf{Q}, t) = \exp(-Q^{*2}/6)$  with  $Q^* = Q(a^2Dt)^{1/4}$ . Here the scattering wave number  $Q$  is normalized by  $(a^2Dt)^{1/4}$ , which is the characteristic length scale defined by the curvilinear diffusion. Due to the tube confinement effect, the spatial correlation of  $F_s(\mathbf{Q}, t)$  exhibits a heavy tail in the reciprocal space. (b) Corresponding self-correlation functions  $G_s(\mathbf{r}, t)$ , obtained by spatial Fourier transform of  $F_s(\mathbf{Q}, t)$ .

viable route to arrive at Eq. (C1) is to consider the segment-dependent self-intermediate scattering function  $F_s(\mathbf{Q}, t; i)$  of the tube model [Eq. (14)] in the limit of  $\mu \gg 1$ . In this case,  $\alpha_p \approx (p - 1/2)\pi$  and  $\mu^2 + \mu \approx \mu^2$ . Additionally, we will concern ourselves with the behavior of only the middle segment ( $s_i = L/2$ ), where the molecular motion is most representative of “reptation.” With these approximations, we have

$$\begin{aligned} F_s(\mathbf{Q}, t) &\approx \sum_{p=1}^{\infty} \frac{2\mu}{\mu^2 + \alpha_p^2} \exp(-4Dt\alpha_p^2/L^2) \\ &\approx \int_1^{\infty} \frac{2\mu}{\mu^2 + \alpha_p^2} \exp(-4Dt\alpha_p^2/L^2) dp \end{aligned}$$

$$\begin{aligned} &\approx \frac{2\mu}{\pi} \int_0^{\infty} \frac{1}{\mu^2 + \alpha_p^2} \exp(-4Dt\alpha_p^2/L^2) d\alpha_p \\ &= \exp(\mathbf{Q}^4 a^2 Dt / 36) \text{erfc}(\mathbf{Q}^2 a \sqrt{Dt} / 6). \end{aligned} \quad (\text{C2})$$

Equation (C1) has an interesting and physically intuitive prediction of the signature of tube confinement in self-dynamics: the spatial correlation of the self-intermediate scattering function  $F_s(\mathbf{Q}, t)$  is a heavy-tailed distribution as a result of the dynamic localization in real space [Fig. 11(a)] [19]. This prediction stands in stark contrast to the behavior of the Rouse model, which is *largely* Gaussian [19]. In the real space, the tube confinement gives rise to an enhanced spatial correlation at small distances [ $r \lesssim (a^2Dt)^{1/4}$ ] and an exponential-like tail at large distances [Fig. 11(b)]. Numerically, the self-correlation function  $G_s(\mathbf{r}, t)$  of the tube model behaves like a Dirac- $\delta$  function near the origin and increases rapidly as  $r$  approaches zero. This prediction is different from that of the slip-spring model (Fig. 8) and also at odds with the results of molecular dynamics simulations (Fig. 2). Such a discrepancy is due to the strict 1D diffusion idea of the original tube model, where the tube is perceived to be impenetrable [19].

Despite the flawed functional form [Eqs. (14) and (C1)] of self-dynamics in the classic tube model, a comparison of theories and simulations (Figs. 2, 6, 8, 11) does seem to suggest some general features of self-dynamics under entanglement constraints: relative to a Gaussian distribution of the same second moment (means-squared displacement), the self-correlation of an entangled polymer is enhanced on small length scales (small relative to the root-mean-square displacement at a given correlation time); additionally, the molecular displacements become more heterogeneous and the self-correlation function is characterized by an exponential-like long tail on large length scales.

- [1] S. Chandrasekhar, Stochastic problems in physics and astronomy, *Rev. Mod. Phys.* **15**, 1 (1943).
- [2] R. Metzler and J. Klafter, The random walk’s guide to anomalous diffusion: A fractional dynamics approach, *Phys. Rep.* **339**, 1 (2000).
- [3]  $G_s(\mathbf{r}, t)$  is also called the self-correlation function or the self part of the van Hove function.
- [4] M. Doi and S. F. Edwards, *The Theory of Polymer Dynamics* (Oxford University Press, Oxford, 1986).
- [5] E. Fischer, R. Kimmich, and N. Fatkullin, NMR field gradient diffusometry of segment displacements in melts of entangled polymers, *J. Chem. Phys.* **104**, 9174 (1996).
- [6] D. Bucknall, S. Butler, and J. S. Higgins, Real-time measurement of polymer diffusion coefficients using neutron reflection, *Macromolecules* **32**, 5453 (1999).
- [7] A. Wischniewski, M. Monkenbusch, L. Willner, D. Richter, and G. Kali, Direct Observation of the Transition from Free to Constrained Single-Segment Motion in Entangled Polymer Melts, *Phys. Rev. Lett.* **90**, 058302 (2003).
- [8] B. Wang, J. Guan, S. M. Anthony, S. C. Bae, K. S. Schweizer, and S. Granick, Confining Potential When a Biopolymer Filament Reptates, *Phys. Rev. Lett.* **104**, 118301 (2010).
- [9] A. Herrmann, B. Kresse, M. Wohlfahrt, I. Bauer, A. Privalov, D. Kruk, N. Fatkullin, F. Fujara, and E. Rössler, Mean square displacement and reorientational correlation function in entangled polymer melts revealed by field cycling  $^1\text{H}$  and  $^2\text{H}$  NMR relaxometry, *Macromolecules* **45**, 6516 (2012).
- [10] P.-G. De Gennes, Reptation of a polymer chain in the presence of fixed obstacles, *J. Chem. Phys.* **55**, 572 (1971).
- [11] K. S. Schweizer, Microscopic theory of the dynamics of polymeric liquids: General formulation of a mode-mode-coupling approach, *J. Chem. Phys.* **91**, 5802 (1989).
- [12] K. S. Schweizer, Mode-coupling theory of the dynamics of polymer liquids: Qualitative predictions for flexible chain and ring melts, *J. Chem. Phys.* **91**, 5822 (1989).
- [13] M. Guenza, Cooperative Dynamics in Unentangled Polymer Fluids, *Phys. Rev. Lett.* **88**, 025901 (2001).
- [14] K. Kremer and G. S. Grest, Dynamics of entangled linear polymer melts: A molecular-dynamics simulation, *J. Chem. Phys.* **92**, 5057 (1990).
- [15] W. Paul and G. D. Smith, Structure and dynamics of amorphous polymers: Computer simulations compared to experiment and theory, *Rep. Prog. Phys.* **67**, 1117 (2004).

- [16] A. E. Likhtman, S. K. Sukumaran, and J. Ramirez, Linear viscoelasticity from molecular dynamics simulation of entangled polymers, *Macromolecules* **40**, 6748 (2007).
- [17] Z. Wang, A. E. Likhtman, and R. G. Larson, Segmental dynamics in entangled linear polymer melts, *Macromolecules* **45**, 3557 (2012).
- [18] H.-P. Hsu and K. Kremer, Static and dynamic properties of large polymer melts in equilibrium, *J. Chem. Phys.* **144**, 154907 (2016).
- [19] J. Ma, J.-M. Y. Carrillo, C. Do, W.-R. Chen, P. Falus, Z. Shen, K. Hong, B. G. Sumpter, and Y. Wang, Spatial correlations of entangled polymer dynamics, *Phys. Rev. E* **104**, 024503 (2021).
- [20] L. Van Hove, Correlations in space and time and Born approximation scattering in systems of interacting particles, *Phys. Rev.* **95**, 249 (1954).
- [21] U. Balucani and M. Zoppi, *Dynamics of the Liquid State*, Oxford Series on Neutron Scattering in Condensed Matter, Vol. 10 (Clarendon Press, Oxford, 1995).
- [22] J.-P. Hansen and I. R. McDonald, *Theory of Simple Liquids: With Applications to Soft Matter* (Academic Press, Oxford, 2013).
- [23] J. Colmenero, F. Alvarez, and A. Arbe, Self-motion and the  $\alpha$  relaxation in a simulated glass-forming polymer: Crossover from Gaussian to non-Gaussian dynamic behavior, *Phys. Rev. E* **65**, 041804 (2002).
- [24] A. Arbe, J. Colmenero, F. Alvarez, M. Monkenbusch, D. Richter, B. Farago, and B. Frick, Non-Gaussian Nature of the  $\alpha$  Relaxation of Glass-Forming Polyisoprene, *Phys. Rev. Lett.* **89**, 245701 (2002).
- [25] J. Baschnagel and F. Varnik, Computer simulations of supercooled polymer melts in the bulk and in confined geometry, *J. Phys.: Condens. Matter* **17**, R851 (2005).
- [26] J.-L. Barrat, J. Baschnagel, and A. Lyulin, Molecular dynamics simulations of glassy polymers, *Soft Matter* **6**, 3430 (2010).
- [27] F. W. Starr, J. F. Douglas, and S. Sastry, The relationship of dynamical heterogeneity to the Adam-Gibbs and random first-order transition theories of glass formation, *J. Chem. Phys.* **138**, 12A541 (2013).
- [28] W. Kob, C. Donati, S. J. Plimpton, P. H. Poole, and S. C. Glotzer, Dynamical Heterogeneities in a Supercooled Lennard-Jones Liquid, *Phys. Rev. Lett.* **79**, 2827 (1997).
- [29] R. Yamamoto and A. Onuki, Heterogeneous Diffusion in Highly Supercooled Liquids, *Phys. Rev. Lett.* **81**, 4915 (1998).
- [30] P. Chaudhuri, L. Berthier, and W. Kob, Universal Nature of Particle Displacements Close to Glass and Jamming Transitions, *Phys. Rev. Lett.* **99**, 060604 (2007).
- [31] A. Heuer and K. Okun, Heterogeneous and homogeneous dynamics in a simulated polymer melt: Analysis of multi-time correlation functions, *J. Chem. Phys.* **106**, 6176 (1997).
- [32] R. Yamamoto and A. Onuki, Entanglements in quiescent and sheared polymer melts, *Phys. Rev. E* **70**, 041801 (2004).
- [33] W. Paul, G. D. Smith, D. Y. Yoon, B. Farago, S. Rathgeber, A. Zirkel, L. Willner, and D. Richter, Chain Motion in an Unentangled Polyethylene Melt: A Critical Test of the Rouse Model by Molecular Dynamics Simulations and Neutron Spin Echo Spectroscopy, *Phys. Rev. Lett.* **80**, 2346 (1998).
- [34] G. D. Smith, W. Paul, M. Monkenbusch, and D. Richter, On the non-Gaussianity of chain motion in unentangled polymer melts, *J. Chem. Phys.* **114**, 4285 (2001).
- [35] A. R. Brás, R. Pasquino, T. Koukoulas, G. Tsolou, O. Holderer, A. Radulescu, J. Allgaier, V. G. Mavrantzas, W. Pyckhout-Hintzen, A. Wischniewski *et al.*, Structure and dynamics of polymer rings by neutron scattering: Breakdown of the Rouse model, *Soft Matter* **7**, 11169 (2011).
- [36] A. R. Brás, S. Gooßen, M. Krutyeva, A. Radulescu, B. Farago, J. Allgaier, W. Pyckhout-Hintzen, A. Wischniewski, and D. Richter, Compact structure and non-Gaussian dynamics of ring polymer melts, *Soft Matter* **10**, 3649 (2014).
- [37] W. Wang, H. Pottmann, and Y. Liu, Fitting b-spline curves to point clouds by curvature-based squared distance minimization, *ACM Trans. Graph.* **25**, 214 (2006).
- [38] T. Springer, *Quasielastic Neutron Scattering for the Investigation of Diffusive Motions in Solids and Liquids* (Springer, Berlin, 1972).
- [39] J. S. Higgins and H. Benoît, *Polymers and Neutron Scattering* (Clarendon Press, Oxford, 1994).
- [40] J. Colmenero and A. Arbe, Recent progress on polymer dynamics by neutron scattering: From simple polymers to complex materials, *J. Polym. Sci. B: Polym. Phys.* **51**, 87 (2013).
- [41] D. Richter, B. Ewen, B. Farago, and T. Wagner, Microscopic dynamics and topological constraints in polymer melts: A neutron-spin-echo study, *Phys. Rev. Lett.* **62**, 2140 (1989).
- [42] P. G. Debenedetti and F. H. Stillinger, Supercooled liquids and the glass transition, *Nature (London)* **410**, 259 (2001).
- [43] L. Berthier, Dynamic heterogeneity in amorphous materials, *Physics* **4**, 42 (2011).
- [44] L. Berthier and G. Biroli, Theoretical perspective on the glass transition and amorphous materials, *Rev. Mod. Phys.* **83**, 587 (2011).
- [45] C. Donati, S. C. Glotzer, P. H. Poole, W. Kob, and S. J. Plimpton, Spatial correlations of mobility and immobility in a glass-forming Lennard-Jones liquid, *Phys. Rev. E* **60**, 3107 (1999).
- [46] P. E. Rouse, A theory of the linear viscoelastic properties of dilute solutions of coiling polymers, *J. Chem. Phys.* **21**, 1272 (1953).
- [47] Numerically, the deviation from the Gaussian behavior is relatively weak in the Rouse model and the commonly employed Gaussian approximation of  $F_s(\mathbf{Q}, t; i)$  can be justified in some cases. See Appendix B for a further discussion.
- [48] M. Doi and S. Edwards, Dynamics of concentrated polymer systems. Part 1.—Brownian motion in the equilibrium state, *J. Chem. Soc., Faraday Trans. 2* **74**, 1789 (1978).
- [49] N. Fatkullin and R. Kimmich, Theory of field-gradient NMR diffusometry of polymer segment displacements in the tube-reptation model, *Phys. Rev. E* **52**, 3273 (1995).
- [50] D. Bedrov, G. Smith, and J. F. Douglas, Structural and dynamic heterogeneity in a telechelic polymer solution, *Polymer* **45**, 3961 (2004).
- [51] Y. Li, M. Kröger, and W. K. Liu, Dynamic structure of unentangled polymer chains in the vicinity of non-attractive nanoparticles, *Soft Matter* **10**, 1723 (2014).
- [52] L.-J. Dai, C.-L. Fu, Y.-L. Zhu, and Z.-Y. Sun, Heterogeneous dynamics of unentangled chains in polymer nanocomposites, *J. Chem. Phys.* **150**, 184903 (2019).
- [53] J. Fan, H. Emamy, A. Chremos, J. F. Douglas, and F. W. Starr, Dynamic heterogeneity and collective motion in star polymer melts, *J. Chem. Phys.* **152**, 054904 (2020).



- [54] W.-S. Xu, J. F. Douglas, and X. Xu, Molecular dynamics study of glass formation in polymer melts with varying chain stiffness, *Macromolecules* **53**, 4796 (2020).
- [55] T. G. Fox Jr. and P. J. Flory, Second-order transition temperatures and related properties of polystyrene. I. Influence of molecular weight, *J. Appl. Phys.* **21**, 581 (1950).
- [56] A. Zaccone and E. M. Terentjev, Disorder-Assisted Melting and the Glass Transition in Amorphous Solids, *Phys. Rev. Lett.* **110**, 178002 (2013).
- [57] J. D. Halverson, W. B. Lee, G. S. Grest, A. Y. Grosberg, and K. Kremer, Molecular dynamics simulation study of nonconcatenated ring polymers in a melt. II. Dynamics, *J. Chem. Phys.* **134**, 204905 (2011).
- [58] J. D. Halverson, W. B. Lee, G. S. Grest, A. Y. Grosberg, and K. Kremer, Molecular dynamics simulation study of nonconcatenated ring polymers in a melt. I. Statics, *J. Chem. Phys.* **134**, 204904 (2011).
- [59] S. Goto, K. Kim, and N. Matubayasi, Effects of chain length on rouse modes and non-Gaussianity in linear and ring polymer melts, *J. Chem. Phys.* **155**, 124901 (2021).
- [60] D. Michieletto and T. Sakaue, Dynamical entanglement and cooperative dynamics in entangled solutions of ring and linear polymers, *ACS Macro Lett.* **10**, 129 (2021).
- [61] A. E. Likhtman, Single-chain slip-link model of entangled polymers: Simultaneous description of neutron spin—Echo, rheology, and diffusion, *Macromolecules* **38**, 6128 (2005).
- [62] G. Tsolou, N. Stratikis, C. Baig, P. S. Stephanou, and V. G. Mavrantzas, Melt structure and dynamics of unentangled polyethylene rings: Rouse theory, atomistic molecular dynamics simulation, and comparison with the linear analogues, *Macromolecules* **43**, 10692 (2010).
- [63] Mean-squared displacement is nothing but the second moment of a self-correlation function.
- [64] C. C. Hua and J. D. Schieber, Segment connectivity, chain-length breathing, segmental stretch, and constraint release in reptation models. I. Theory and single-step strain predictions, *J. Chem. Phys.* **109**, 10018 (1998).
- [65] Y. Masubuchi, J.-I. Takimoto, K. Koyama, G. Ianniruberto, G. Marrucci, and F. Greco, Brownian simulations of a network of reptating primitive chains, *J. Chem. Phys.* **115**, 4387 (2001).
- [66] M. Doi and J.-i. Takimoto, Molecular modelling of entanglement, *Philos. Trans. A* **361**, 641 (2003).
- [67] Z. Shen, J. Ma, J.-M. Y. Carrillo, W.-R. Chen, B. G. Sumpter, and Y. Wang, Spatiotemporal mapping of mesoscopic liquid dynamics, *Phys. Rev. E* **103**, 022609 (2021).
- [68] P. Santangelo and C. Roland, Molecular weight dependence of fragility in polystyrene, *Macromolecules* **31**, 4581 (1998).
- [69] J. Hintermeyer, A. Herrmann, R. Kahlau, C. Goiceanu, and E. Rossler, Molecular weight dependence of glassy dynamics in linear polymers revisited, *Macromolecules* **41**, 9335 (2008).
- [70] K. Kunal, C. G. Robertson, S. Pawlus, S. F. Hahn, and A. P. Sokolov, Role of chemical structure in fragility of polymers: A qualitative picture, *Macromolecules* **41**, 7232 (2008).
- [71] C. Bennemann, J. Baschnagel, and W. Paul, Molecular-dynamics simulation of a glassy polymer melt: Incoherent scattering function, *Eur. Phys. J. B* **10**, 323 (1999).
- [72] M. Aichele and J. Baschnagel, Glassy dynamics of simulated polymer melts: Coherent scattering and van Hove correlation functions, *Eur. Phys. J. E* **5**, 229 (2001).
- [73] R. Yamamoto and A. Onuki, Dynamics and rheology of a supercooled polymer melt in shear flow, *J. Chem. Phys.* **117**, 2359 (2002).
- [74] M. Bernabei, A. J. Moreno, and J. Colmenero, Dynamic Arrest in Polymer Melts: Competition between Packing and Intramolecular Barriers, *Phys. Rev. Lett.* **101**, 255701 (2008).
- [75] W.-S. Xu, J. F. Douglas, and K. F. Freed, Influence of cohesive energy on the thermodynamic properties of a model glass-forming polymer melt, *Macromolecules* **49**, 8341 (2016).
- [76] Z. Yang, X. Xu, and W.-S. Xu, Influence of ionic interaction strength on glass formation of an ion-containing polymer melt, *Macromolecules* **54**, 9587 (2021).
- [77] C. Angell, Relaxation in liquids, polymers and plastic crystals—Strong/fragile patterns and problems, *J. Non-Cryst. Solids* **131**, 13 (1991).
- [78] R. Böhmer, K. Ngai, C. A. Angell, and D. Plazek, Non-exponential relaxations in strong and fragile glass formers, *J. Chem. Phys.* **99**, 4201 (1993).
- [79] Y. Ding, V. Novikov, A. Sokolov, A. Cailliaux, C. Dalle-Ferrier, C. Alba-Simionesco, and B. Frick, Influence of molecular weight on fast dynamics and fragility of polymers, *Macromolecules* **37**, 9264 (2004).
- [80] G. Yatsenko, E. J. Sambriski, M. A. Nemirovskaya, and M. Guenza, Analytical Soft-Core Potentials for Macromolecular Fluids and Mixtures, *Phys. Rev. Lett.* **93**, 257803 (2004).
- [81] A. Rahman, K. S. Singwi, and A. Sjölander, Theory of slow neutron scattering by liquids. I, *Phys. Rev.* **126**, 986 (1962).
- [82] J. P. Boon and S. Yip, *Molecular Hydrodynamics* (Dover Publications, New York, 1991).
- [83] R. Zorn, Deviation from Gaussian behavior in the self-correlation function of the proton motion in polybutadiene, *Phys. Rev. B* **55**, 6249 (1997).
- [84] Z. Wang and R. G. Larson, Constraint release in entangled binary blends of linear polymers: A molecular dynamics study, *Macromolecules* **41**, 4945 (2008).
- [85] A. Maitra and A. Heuer, Cation Transport in Polymer Electrolytes: A Microscopic Approach, *Phys. Rev. Lett.* **98**, 227802 (2007).
- [86] D. Diddens, A. Heuer, and O. Borodin, Understanding the lithium transport within a Rouse-based model for a PEO/LiTFSi polymer electrolyte, *Macromolecules* **43**, 2028 (2010).
- [87] F. W. Starr, T. B. Schröder, and S. C. Glotzer, Molecular dynamics simulation of a polymer melt with a nanoscopic particle, *Macromolecules* **35**, 4481 (2002).
- [88] R. Picu and A. Rakshit, Dynamics of free chains in polymer nanocomposites, *J. Chem. Phys.* **126**, 144909 (2007).
- [89] Z. Zheng, F. Li, J. Liu, R. Pastore, G. Raos, Y. Wu, and L. Zhang, Effects of chemically heterogeneous nanoparticles on polymer dynamics: Insights from molecular dynamics simulations, *Soft Matter* **14**, 1219 (2018).
- [90] E. Y. Lin, A. L. Frischknecht, and R. A. Riggleman, Chain and segmental dynamics in polymer–nanoparticle composites with high nanoparticle loading, *Macromolecules* **54**, 5335 (2021).
- [91] <http://lammps.sandia.gov>.
- [92] S. Plimpton, Fast parallel algorithms for short-range molecular dynamics, *J. Comput. Phys.* **117**, 1 (1995).
- [93] W. M. Brown, P. Wang, S. J. Plimpton, and A. N. Tharrington, Implementing molecular dynamics on hybrid high

- performance computers—Short range forces, *Comput. Phys. Commun.* **182**, 898 (2011).
- [94] J. D. Weeks, D. Chandler, and H. C. Andersen, Role of repulsive forces in determining the equilibrium structure of simple liquids, *J. Chem. Phys.* **54**, 5237 (1971).
- [95] T. C. O'Connor, A. Hopkins, and M. O. Robbins, Stress relaxation in highly oriented melts of entangled polymers, *Macromolecules* **52**, 8540 (2019).
- [96] R. Auhl, R. Everaers, G. S. Grest, K. Kremer, and S. J. Plimpton, Equilibration of long chain polymer melts in computer simulations, *J. Chem. Phys.* **119**, 12718 (2003).
- [97] W.-S. Xu, J.-M. Y. Carrillo, C. N. Lam, B. G. Sumpter, and Y. Wang, Molecular dynamics investigation of the relaxation mechanism of entangled polymers after a large step deformation, *ACS Macro Lett.* **7**, 190 (2018).
- [98] G. S. Grest, Communication: Polymer entanglement dynamics: Role of attractive interactions, *J. Chem. Phys.* **145**, 141101 (2016).
- [99] H. C. Öttinger, *Stochastic Processes in Polymeric Fluids: Tools and Examples for Developing Simulation Algorithms* (Springer, Berlin, 1996).
- [100] To be consistent with the notation of Likhtman, here  $N$  stands for the number of bonds in the constrained Rouse chain. The total number of beads in a chain there is  $N + 1$ .
- [101] P.-G. De Gennes, Quasi-elastic scattering of neutrons by dilute polymer solutions: I. Free-draining limit, *Phys. Phys. Fiz.* **3**, 37 (1967).